

CLIMATE-INDUCED MOBILIZATION OF RARE EARTH ELEMENTS IN HIGH
ALTITUDE STREAMS, COLORADO: POTENTIAL ROLE OF COMPLEXATION IN
HYDROUS METAL OXIDE PRECIPITATION

by

Nicole Kathleen Schneider Brooks

B.S., The City University of New York at Brooklyn College, 2017

A thesis submitted to the
Faculty of the Graduate School of the
University of Colorado in partial fulfillment
of the requirement for the degree of
Master of Science in Department of Environmental Engineering
2023

Committee Members:

Dr. Diane M. McKnight

Dr. Tom Marchitto

Dr. Anthony Straub

ABSTRACT

Brooks, Nicole K.S. (M.S., Environmental Engineering)

Climate-Induced Mobilization of Rare Earth Elements in High Altitude Streams, Colorado:
Potential Role of Complexation in Hydrous Metal Oxide Precipitation

Thesis directed by Dr. Diane M. McKnight

Pyrite weathering, the biogeochemical process creating acid rock drainage (ARD) and acid mine drainage (AMD), is commonly associated with the mobilization of trace metals and eventual precipitation of hydrous metal oxides. Drier conditions attributed to a warming climate have accelerated this process. The chemical parameters for pyrite weathering generate concentrations that mobilize various metals, including rare earth elements (REEs). Recently, an increase in REE concentration was discovered in a tributary leading to the Dillon Reservoir, CO- the source of drinking water for Denver, Colorado. The humic fraction of dissolved organic matter (DOM) can form complexes with REEs and can also be sorbed by hydrous metal oxides. To study this relationship and the fate and transport of REEs I chose five locations in the Colorado Mineral Belt with distinct biogeochemical environments. These locations vary in dominant types of hydrous metal oxides, DOM sources, such as above tree lines, subalpine forests or wetlands, and known REE concentrations in country rock or water. To gain an understanding of the DOM-REE relationship I used synoptic sampling to (1) identify geochemical parameters, particularly REEs, sum and individual concentrations, within streamwater and flocculant found on the streambed (2) used these geochemical parameters to assess the connections between changes in REE-DOM complexes and their sorption onto hydrous metal oxides. DOM has some control on the REE sorption, but the dominant control is the precipitation and concentration of hydrous Al oxides. REEs are preferentially sorbed with Al precipitates over Fe precipitates. This research advances

the understanding of how REEs behave in aqueous environments and will be useful in addressing issues related to increasing REEs concentrations in the Colorado Mineral Belt. This research is particularly relevant to adaptation to climate change driven changes in water quality because there are currently no drinking water standards regarding REEs.

ACKNOWLEDGEMENTS

First and foremost I would like to acknowledge my advisor, Dr. Diane McKnight, for her incredible and unwavering support both academically and personally throughout this journey. I want to thank the National Science Foundation INTERN Program which made all of this possible. This program gave me the opportunity to consult and work with Dr. Rory Cowie of Alpine Water Resources, which was particularly helpful when surveying California Gulch. I want to thank the entire INSTAAR office team for helping me navigate the award and budget process. Thank you to Dr. Tom Marchitto who diligently and patiently led me through the process of obtaining ICP-MS metal data with tricky samples. Thank you to my thesis committee, Dr. Diane McKnight, Dr. Tom Marchitto, and Dr. Anthony Straub for their knowledgeable input and time. I want to thank my incredible UROP students, Ryan Hoak and Kiersten Maxwell, who fearlessly followed me into the field only to lead and encourage me up every mountain. I want to thank Stefan Petersen, Marisa Repasch, Wendy Roth, Kathy Welsch, and Jimmy McCutchan, for their guidance and assistance with lab analysis.

Thank you to the entire McKnightmare lab group, friends, and EVEN cohort for supporting me and reminding me to take a break for a beer or ice cream. Thank you to friends and family who took time out of their day to care for Adi-Lou so I could focus and study. Huge thank you to my nanny, Lindsey Hughes, for staying late and giving me a good laugh when I needed it most. The biggest thank you is to my partner, Charlie, who was always there to remind me I could do this when I felt like I couldn't. Your understanding and patience continue to ground me and support me to pursue my ambitions. Thank you to my little bug, Adi-Lou for

understanding when “Mama, at school,” and giving me the best snuggles. Your giggle inspires me every day.

CONTENTS

1.0 INTRODUCTION	1
1.1 The Process of Pyrite Weathering	2
1.2 Hydrous Metal Oxides and Dissolved Organic Material	2
1.3 Rare Earth Elements	4
1.4 Zinc and REEs	6
1.5 Environmental Problems of ARD and AMD	6
1.6 Purpose of Investigation	7
2.0 METHODS	9
2.1 Sampling Locations Descriptions and Justification	23
2.2 Field measurements	23
2.3 Lab Analysis	24
2.4 Theory	26
3.0 RESULTS	29
3.1 Iron Hill	29
3.2 Tributary 2095	30
3.3 Snake River - Deer Creek Confluence	33
3.4 Little Sayres Gulch	38
3.5 Paradise Creek	40
3.6 California Gulch	42
3.7 Flocculant Fe/Al and total REEs	44
3.8 Water Fluorescence Index and Flocculant Carbon/Nitrogen Ratio	45
4.0 DISCUSSION	47
4.1 Water Chemistry	47
4.2 Flocculant Chemistry	52
4.3 Aluminum, Iron, and Total REE Relationships	55
4.4 Fluorescence Index and Carbon/Nitrogen Ratio	57
4.5 Variable Weight Percentages of Flocculant	61
5.0 CONCLUSIONS	63
6.0 REFERENCES	64
7.0 APPENDIX AND SUPPLEMENTARY MATERIAL	71

LIST OF TABLES

Table 1. Values used for SN-DC Comparison	44
Table 2. Flocculant data compared to water pH and dissolved Fe content	68
Table 3. Field and Single water measurements	79
Table 4. Water REE concentrations	81
Table 5. Water Trace Metal Concentrations	82
Table 6. Flocculant Chemistry	84
Table 7. Cerium Anomaly Standard Values for PAAS and PPREE1	86
Table 8. Calculated Values for Site Ce* Standardization	86
Table 9. Cerium anomaly all methods for water and flocculant	88
Table 10. Fluorescence Index	90

LIST OF FIGURES

Figure 1. Transport and removal relationship between DOM, trace metals, and oxides at the SN-DC confluence.	12
Figure 2. Map of sampling locations within the Colorado Mineral Belt	17
Figure 3. Iron Hill	18
Figure 4. Map of the Iron Hill area with sampling sites.	19
Figure 5. Tributary 2095	20
Figure 6. Overview of Tributary 2095 and sampling sites.	21
Figure 7. Spatial relationship between Tributary 2095 and the SN-DC confluence.	21
Figure 8. SN-DC confluence.	22
Figure 9. Overview of the SN-DC Confluence.	23
Figure 10. Overview of Little Sayres Gulch	24
Figure 11. Overview of Little Sayres Gulch study area indicating sample sites.	25
Figure 12. Paradise Creek	26
Figure 13. Overview of PC and sampling sites.	27
Figure 14. California Gulch	28
Figure 15. Overview of California Gulch and sampling sites.	30
Figure. 16 Water chemistry of Iron Hill	36
Figure 17. Water chemistry of 2095.	37

Figure 18. Flocculant chemistry of tributary 2095.	38
Figure 19. Snake River - Deer Creek temporal comparative available data.	40
Figure 20. SN-DC water sampling sites	41
Figure 21. Flocculant data comparison between 1980 and 2022.	43
Figure 22. Overview of flocculant sample sites A-D.	44
Figure 23. Water chemistry Little Sayres Gulch.	45
Figure 24. Flocculant chemistry of Little Sayres Gulch.	46
Figure 25. Water chemistry of Paradise Creek.	47
Figure 26. Paradise Creek flocculant chemistry.	48
Figure 27. California Gulch water chemistry.	49
Figure 28. Flocculant chemistry of California Gulch.	50
Figure 29. Relating Al/Fe to total REEs.	52
Figure 30. All sites compare the water fluorescence index and flocculant C/N ratio.	53
Figure 31. Cerium anomaly (Ce*) compared to the Nd concentrations.	57
Figure 32. Distribution of total REE concentrations in each sample.	61
Figure 33. Sample distribution of percent Al concentrations.	61
Figure 34. The sample frequency of log ratio of Al/Fe.	62
Supplementary Material	65

EQUATIONS

Eq. 1. Raman Correction	32
Eq. 2. Fluorescence Index	32
Eq. 3. Normalization of REE in the sample to standard	33
Eq. 4. Cerium Anomaly (Ce*) Calculation	34

NOMENCLATURES

Fluorescence Index (F.I.)

Raman Unit (R.U.)

Rare earth elements (REE)

Acid Rock Drainage (ARD)

Acid Mine Drainage (AMD)

Max Contaminant Levels (MCL)

Dissolved Organic Matter (DOM)

Dissolved Organic Carbon (DOC)

Little Sayres Gulch (LS)

Paradise Creek (PC)

Iron Hill (IH)

Tributary 2095 (Tib 2095; 2095)

California Gulch (CG)

Deer Creek (DC)

Snake River (SN)

Deldorado Creek (D)

Cebolla Creek (C)

Beaver Creek (BC)

1.0 INTRODUCTION

Encompassing a large portion of the Colorado Rocky Mountains, the Colorado Mineral belt is a rich host to sulfide minerals. When exposed to oxidation these minerals create sulfuric acid which leaches trace metals from the country rock. This process is known as pyrite weathering. This biogeochemical process creates acid rock drainage (ARD) and acid mine drainage (AMD) and is commonly associated with the mobilization of leached trace metals.

Drier summer conditions associated with a warming climate have accelerated this process by exposing more pyrite to oxidation (Todd et al., 2012; Crouch et al., 2013; Manning et al., 2013). Evaluation of data from 1948-2000 indicates snowmelt is 1-4 weeks earlier in the Sierra Nevada mountains, the Rocky Mountains, and the Pacific Northwest (Stewart et al., 2005). The earlier the snowmelt the longer the summer dry periods creating lower water tables and exposing more dry surface area in soils allowing for oxidation (Todd et al., 2012). Shifts in summer temperatures could also be a mechanism for increased solute concentrations. Warmer temperatures increase evapotranspiration and the transfer of water to the atmosphere resulting in more intense rainfall (Todd et al., 2012; Zarroca et al., 2021). Longer drier summers and rain intensity increasing with more time between events causes increased groundwater residence time resulting in more weathering and metal leaching. Dry periods and longer low flow periods result in higher average concentrations of metal, sulfate, and acidity in stream flow. Crouch et. al. (2013) found pH was lower during summer periods because the decrease in stream flow increased concentrations. Shallow acidic groundwater can be flushed by fresh infiltration (Nordstrom, 2009). The first major rainstorm following a prolonged dry period can result in a “first flush” event causing a spike in concentrations in stream flow indicating groundwater residence time greatly affects concentrations.

1.1 The Process of Pyrite Weathering

In the CO Mineral Belt, sulfidic minerals (e.g. pyrite (FeS_2)) are exposed to chemical weathering by oxygen, and water (Todd et al., 2012). The pyrite weathering process is microbially mediated and results in the mobilization of H^+ ions, SO_4^- and metals (e.g. typically Fe, Al, Zn, Cu, Cd, Mn). The initial oxidation of pyrite releases acid into the water (E1) (Singer & Stumm, 1970). This process initiates the propagation cycle (E2) where ferrous iron (Fe^{2+}) is oxidized to ferric iron (Fe^{3+}) which then reacts with pyrite producing ferrous iron (Fe^{2+}) resulting in more protons released and more acidity. Oxidants in this system are oxygen and Fe^{3+} . The reduction of Fe^{3+} is independent of whether oxygen is present. In acidic conditions, abiotic oxidation reactions of ferrous iron is slow and the oxidation of ferrous iron to ferric iron is a microbial mediation performed by *Thiobacillus ferrooxidans*, a gram-negative acidophilic chemolithoautotroph (Harahuc et al., 2000). This bacterial taxon grows best in acidic conditions and uses the oxidation of ferrous iron, sulfur, and reduced sulfur compounds as energy for growth. In a sterile lab environment, *T. ferrooxidans* can accelerate the oxygenation of Fe^{2+} reaction by a factor 10^6 (Singer & Stumm, 1970). The experimentally observed rate of pyrite oxidation relies mostly on the surface area of the sample and the initial concentration of the oxidizing agent (Bierens de Haan, 1991).

1.2 Hydrous Metal Oxides and Dissolved Organic Material

Following the leaching of metals by the aforementioned processes, based on concentrations cations become hydrated by water to move downstream. It is important to note that mobilized metals be present as free metal ions and as dissolved metal hydroxide species, and form precipitates furthering the acidity (Washington, 2016). In the Snake River-Deer Creek (SN-DC)

confluence, in the mixing zone of the low pH (<3.5) Snake River and the pristine Deer Creek (pH >6) the pH rises and the hydrous metal oxides precipitate out onto the streambed (Theobald et al., 1963).

Dissolved organic matter (DOM) is removed via the sorption onto hydrous metal oxides, like aluminum and iron (Figure 1; McKnight et al., 1992). The two reactive fractions in this process are fulvic acids and hydrophilic acids which have heterogeneous and diverse characteristics with an affinity for oxide surfaces. In high-altitude streams, Dissolved Organic Carbon (DOC) originates in upper soil horizons and fluxes into streams during spring snow melt (Brooks et al., 1999).

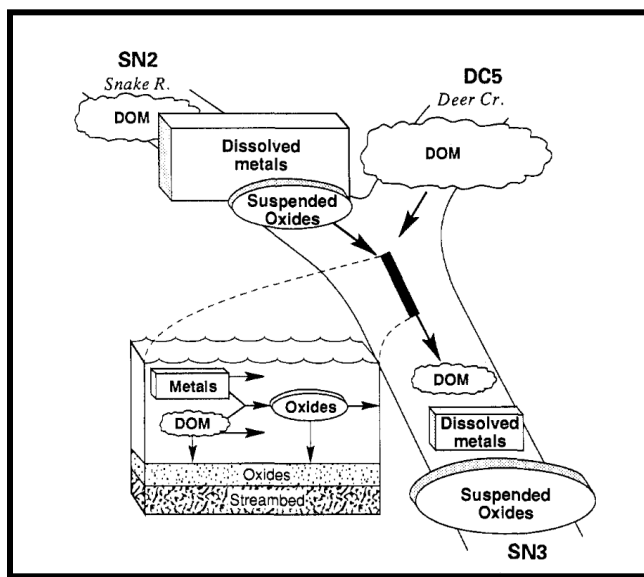


Figure 1. McKnight et. al, 1992 detail the transport and removal relationship between DOM, trace metals, and oxides at the SN-DC confluence.

These variable and seasonal flushes of DOC can form complexes with trace metals and subsequently interfere with concentrations by acting as a sink for increased metal concentrations during snowmelt. Al concentrations were observed to vary seasonally with lower concentrations. Whereas, Fe concentrations can vary diurnally through a solution-based photoreduction process of ferric iron oxide to ferrous iron (David and David, 1976; McKnight & Bencala, 1988). This

process is dependent on UV radiation and can vary with shading or seasonal snow cover. Ferrous iron becomes the major iron species during periods of sunshine because of the dissolution of hydrous ferric iron oxides existing on the stream bed. Further investigation of this transient storage found areas with forest shade cover in downstream reaches showed a substantial loss of iron (McKnight & Bencala, 1988). The quantum yield of this process increases at lower pH values. McKnight and Bencala (1988), found increases in ferrous iron during the early morning hours before sunrise. McKnight et al. (1990), used a lithium tracer and sulfuric acid in the Snake River to lower the pH and found there was an unexpected increase in Fe. This was a response attributed to Fe concentrations and photoreduction interactions.

1.3 Rare Earth Elements

REEs consist of 15 elements naturally found in trace amounts in biological systems, in soil (based on their parent rock composition), and in aquatic environments. Rare earth elements (REEs) have atomic numbers 57-71 and 39 (USGS Mineral Resources Program, 2014). Atomic number 39 (Yttrium, Y) is included because this element has similar chemical and physical properties. Yttrium also typically occurs in the same deposits as REEs. While REEs are called “Rare” earth elements, they are more abundant than copper, gold, and platinum in Earth’s crust. The term “rare” was added to these elements because they cannot be changed by heat and were relatively rare compared to other elements (e.g. Earthy elements like lime and magnesia) of the 18th/19th century.

REEs assimilate into minerals during igneous rock crystallization. They commonly are found within the silicate crystallization of feldspars, pyroxenes, olivines, and amphiboles. As the magma crystallizes REE concentration in the residual magma increases. All REEs are trivalent or

have an electron valence of three (Olías et al., 2018). In addition, REEs can fit into minerals as major or minor constituents and multiple REEs can occur in the same mineral. REEs in aquatic environments can form complexes with cations, anions and DOC, and lignans (organic and inorganic). Most importantly, REEs form strong complexations with fluoride, sulfate, phosphate, carbonate, and some hydroxides. The REE complexation with sulfate is a result of the carbonate preference for H^+ over REEs, so REEs will complex with sulfate to form $(REE)SO_4^+$. However, carbonate-REE complexes are highly insoluble and will only be complex at a higher pH. The complexes of REEs and phosphate are highly insoluble and less dominant in natural waters in this state. Fe/Mn-OH complexes may bind or enclose some REEs. The primary driver of REEs and their sorption behavior are pH-driven (Malhotra et al., 2020). pH competes for binding sites and affects the surface charge. Low pH and high concentrations of La cause REEs to have very different behaviors. As pH lowers the complexation of REEs decreases and REEs become more dissolved. When pH decreases to 3 REEs tend to behave conservatively in river systems (Olías et al., 2018). REEs complex with hydrous oxides and organic matter. Verplanck et al. (1999), noticed total REE concentrations remain conservative until a pH of 4.3 is reached when compared to the conservative SO_4 concentrations. The removal of REEs from the samples was observed with Al either by coprecipitation or adsorption onto Al oxide colloids.

REEs contain unique magnetic and optical properties. The use of REEs in industrial, electronic, and medical industries has increased in recent years. Magnetically they have stronger magnetic properties per unit weight than other types of magnets. Optically, REEs are widely used in the glass industry to polish glass or as an additive to provide color and other special optical properties. Lanthanum (57) attributes up to 50% of digital and cell camera lenses.

Recent studies have increasingly shown the biotoxicity of REEs. Residents in close proximity to REE mines in China have shown bioaccumulation of REEs in blood, brain, and bones. Other studies have shown detailed adverse effects on living biological systems. To humans specifically, REEs effects include male sterility, anti-testicular effects, oxidative stress, neurodegenerative diseases like Alzheimer's or Parkinson's, changes in mitotic activity, cytogenetic anomalies, and fibrotic tissue injury (e.g. Malhotra et al., 2020; Olías et al., 2018; Pagano, 2017; Pagano et al., 2015).

1.4 Zinc and REEs

Zinc is a conservative metal within stream systems. It is not affected by pH-dependent sorption and precipitation reactions. This makes it a viable conservative tracer of ARD sources. Petach, 2022 Ph.D. thesis collected temporal data on numerous sites in the Colorado Mineral Belt. Previous studies have shown an almost four-fold increase in zinc in the Snake watershed in the last 20 years (Crouch et al., 2009; 2012). The source of eighty percent of the zinc contribution was from Tributary 2095. Further study of this site and streams within the same Snake River Watershed indicated the behavior of REEs was similar to the increasing trend of zinc (Rue and McKnight, 2021). The relationship between REE and zinc behavior could serve as a strong predictor of water chemistry and streams affected by ARD and AMD.

1.5 Environmental Problems of ARD and AMD

Many environmental and ecological issues are associated with AMD and ARD. The low acidity can create acidic flushes (Nordstrom, 2009). These acidic flushes are rapid events from sudden rainstorms that instigate large fish kills with deaths estimated at up to 100,000 fish during one

storm event. This acidity can affect the aquatic ecosystems but so can the mobilized trace metals. High concentrations of dissolved zinc are lethal to aquatic organisms particularly when considering exposure time (Skidmore, 1964). Concentrations of just 30 ppm of zinc sulfate has been shown to kill mature sticklebacks (*Gasterosteus aculeatus*) in just over 5 hours attributed to the cellular breakdown of gills clogging them in mucus resulting in suffocation. Cadmium in aquatic environments is more toxic in environments with a lower dose for a longer period when compared to lead (Spehar, 1978). Lead exposure results in greater than LD₅₀ within 4 days with a concentration of 136 ppb. The LD₅₀ of cadmium exposed amphipods in 28 days. REEs have been shown to bioaccumulate in macroinvertebrates (Amyot et al., 2017; MacMillan et al., 2017; Malhotra et al., 2020).

In addition, the mobilization of trace metals can contaminate drinking water, and corrode and erode infrastructure (*Mining and Water Quality*, n.d.). In West Virginia, the cost of remediation efforts for AMD is estimated at \$5-15 billion.

While the complexation of hydrous metal oxides and DOM have been well documented, the role of REEs within this system has yet to be well understood. The Environmental Protection Agency (EPA) has water quality maximum contaminant levels (MCL) for over 90 contaminants (e.g. Lead, Pb, 0.0 MCL; Cadmium, Cd, 0.005 mg/L) (US EPA, 2015). However, not one REE is listed.

1.6 Purpose of Investigation

Investigation of these concepts and understanding the fate and transport of REEs to determine their role in complexation with DOM and subsequent sorption by hydrous metal oxides began by

selecting sites within the Colorado Mineral Belt. The goals of site selection for synoptic studies were to find sites with:

- 1) varying degrees of AMD and/or ARD
- 2) first-order streams with access above the treeline
- 3) variable inputs of dissolved organic matter input (e.g. wetland, subalpine forest)
- 4) different dominant hydrous metal oxides

Five uniquely different sites within the Colorado Mineral Belt have been chosen to answer this question with three main objectives. (1) identify geochemical parameters, particularly REE, summed and individual concentrations (2) use the geochemical parameters to assess the connection between changes in REE concentration and DOM concentration. (3) Compare site selections with previous sample data, if available, to determine temporal changes of objectives 1 and 2.

2.0 METHODS

2.1 Sampling Locations Descriptions and Justification

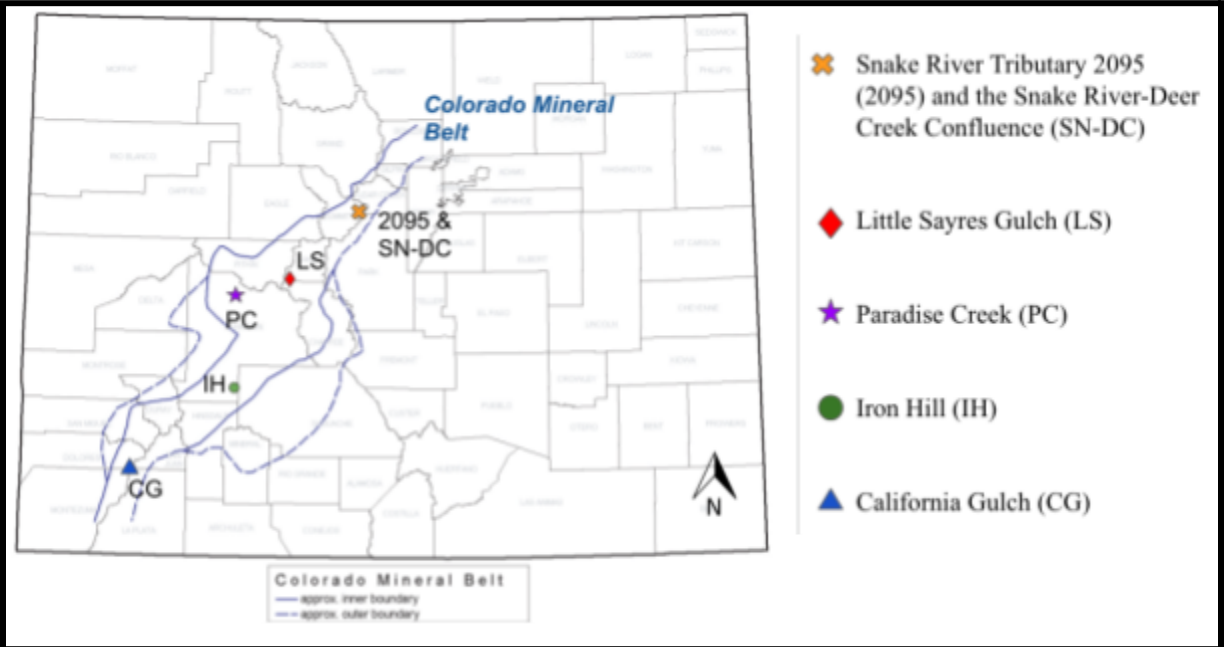


Figure 2. An overview map of sampling locations within the Colorado Mineral Belt adapted from Wilson and Sims, 2003.

Iron Hill, Colorado

Iron Hill, Colorado, (IH) is a large carbonatite deposit surrounded by three streams near Powderhorn, CO (Figure 3A.) at an elevation of 8,300 ft. Carbonatite rock is a rare intrusive or extrusive carbonate igneous rock (USGS Mineral Resources Program, 2014, Van Gosen, 2009). These rocks consist of 50 percent or more carbonate minerals (e.g. calcite, dolomite) and are formed by magmatic or metasomatic processes. The carbonate minerals do not form because of the associated alteration processes. Instead, carbonatites crystallize from magma super-saturated with carbon dioxide and calcium. While there are many theories about the formation of



Figure 3. A) Overview photo of Iron Hill from Beaver Creek 2 (BC2). B) UROP students Kiersten Maxwell (left) and Ryan Hoak (right) sampling BC3. C) Deldorado Creek

carbonatites the most popular theory is the partial melting of peridotites in the upper mantle leads to their formation. There are more than 500 carbonatite deposits globally but only six are mined for REEs despite they have the highest concentration of REEs of all igneous rocks. Iron Hill carbonatite has a rock concentration of 910 ppm Ce and 1,960 ppm total REE. The adjacent pyroxene unit has a rock concentration of 510 ppm Ce 1,240 ppm total REE. Two streams border Iron Hill: Beaver Creek in the south and Deldorado Creek in the north, both confluence with Cebolla Creek. Five sites were sampled along Beaver Creek (Figure 3A, 4; BC1-BC5), two in Cebolla Creek (C1-C2) (Figure 4), and one in Deldorado Creek (D1) (Figure 3C, 4). This location was chosen for the known high concentrations of REEs within the rock and for its

elevation. Iron Hill area is below treeline at an elevation of 8,300 ft . The consistency of organic matter with stream in contact with REEs rich deposits makes this location a control in my study.

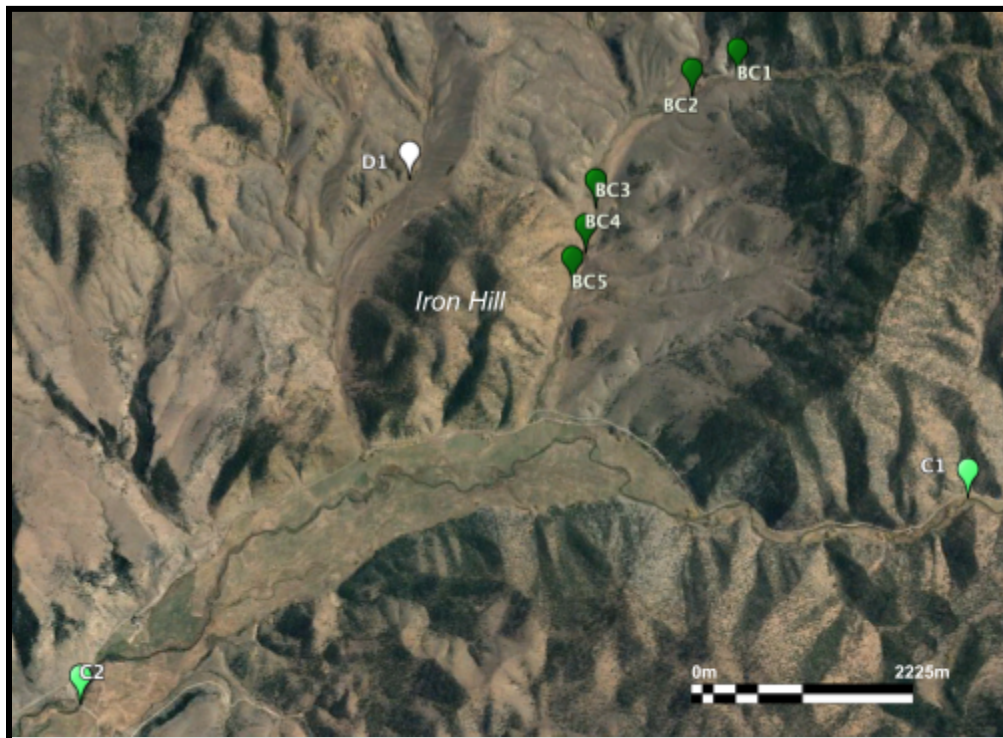


Figure 4. Map of the Iron Hill area with sampling sites.

Tributary 2095, CO

Tributary 2095 (Trib 2095) is a high-altitude stream at 11,483 ft that flows into the Snake River 1.55 km before the heavily studied Snake River - Deer Creek confluence (Figure 7). This tributary is not impacted by mining (Rue & McKnight, 2021). Tributary 2095 has noticeably high iron concentrations with rust colored water (Figure 5 A-C). It has a pH of 3. Recently, Rue and McKnight, 2021, found the highest REE concentrations ranged from 6-40 $\mu\text{g/L}$ in Trib 2095 when measured in 2009 during a drought with record low flows. Distribution of REEs shifted

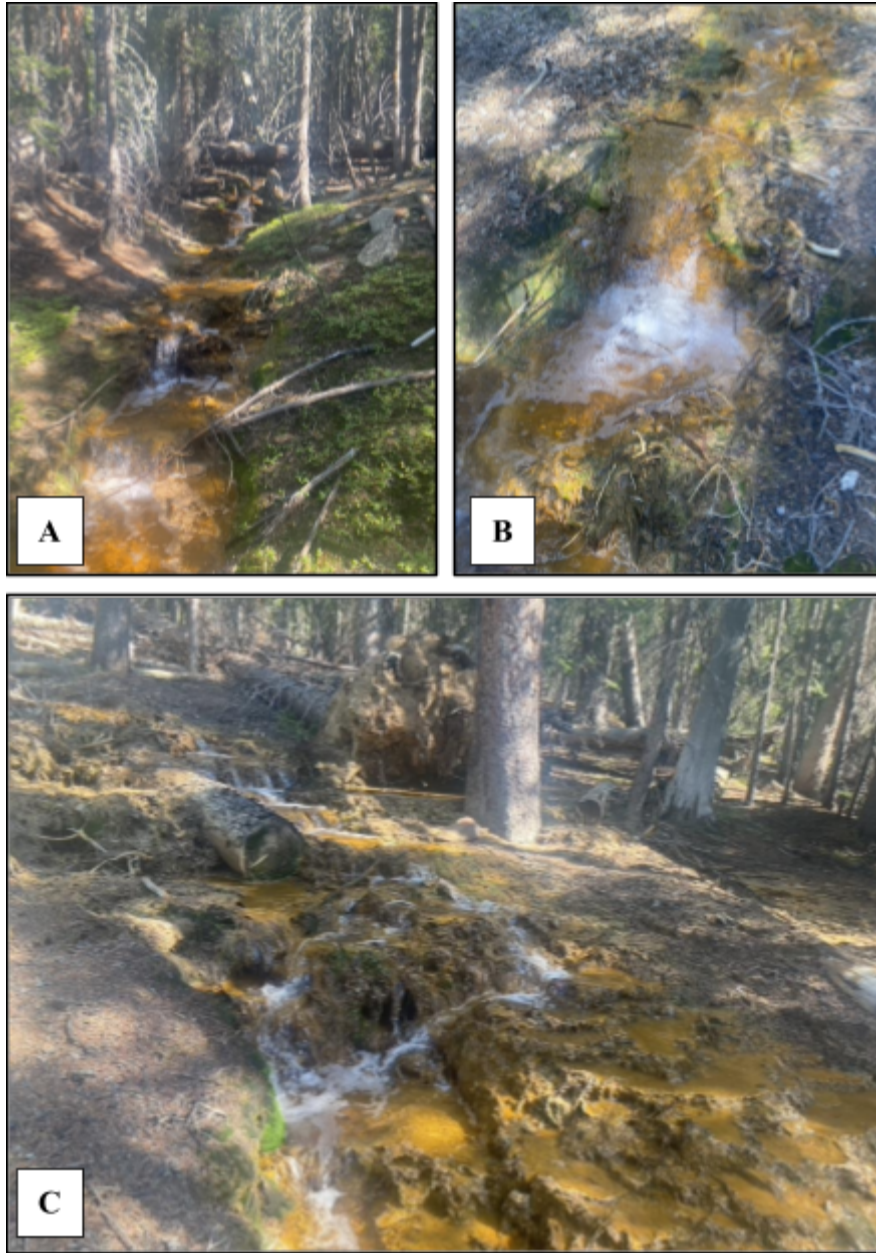


Figure 5. A) Overview of Trib 2095 B) Close up of spatial vegetation and stream bed. C) Fe precipitation on the stream bed.

between drought years and those with more normal flow. These concentrations increased 2-fold two years later. Trib 2095 originates above the treeline and flows through a subalpine forest before its confluence with the Snake River (Figure 6). Eight sites were sampled to correspond to the same sampling sites in Crouch et al. (2012) and the samples collected by Crouch in October

2009 were subsequently analyzed for REEs by Rue MS thesis in 2012, and published in Rue & McKnight (2021). Synoptical sampling of this site allows for comparison to the data analyzed by Rue in 2012. This location was chosen because of previous studies and accessibility to above treeline.

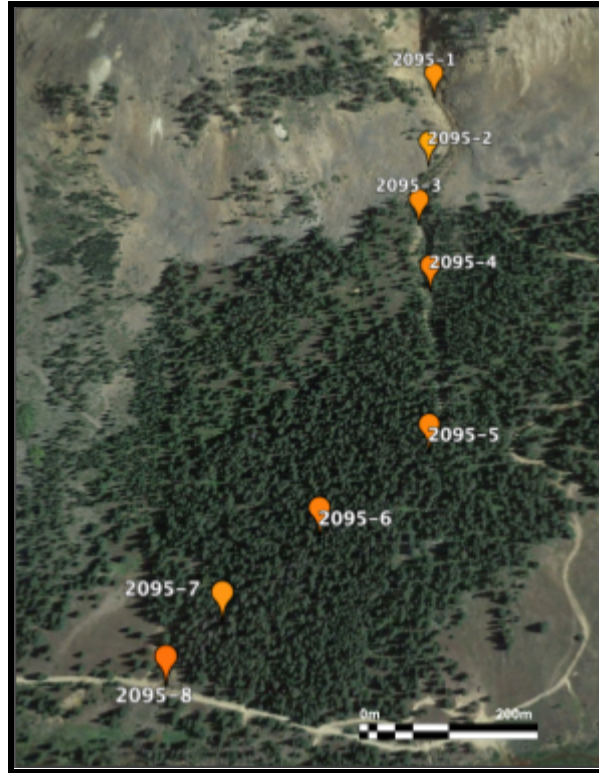
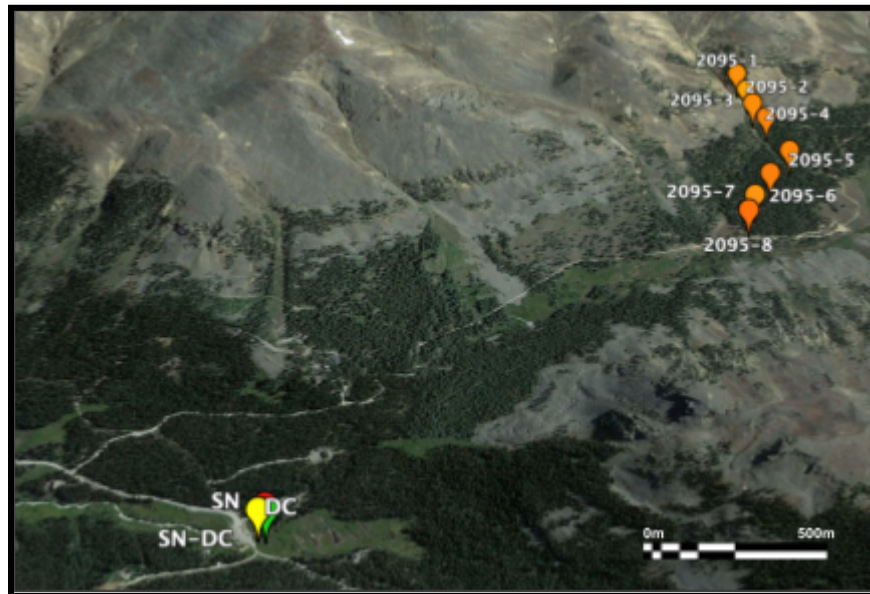


Figure 6. (above) Overview of Tributary 2095 and sampling sites. Figure 7. (below) Overview of the spatial relationship between Tributary 2095 and the SN-DC confluence.



Snake River - Deer Creek Confluence

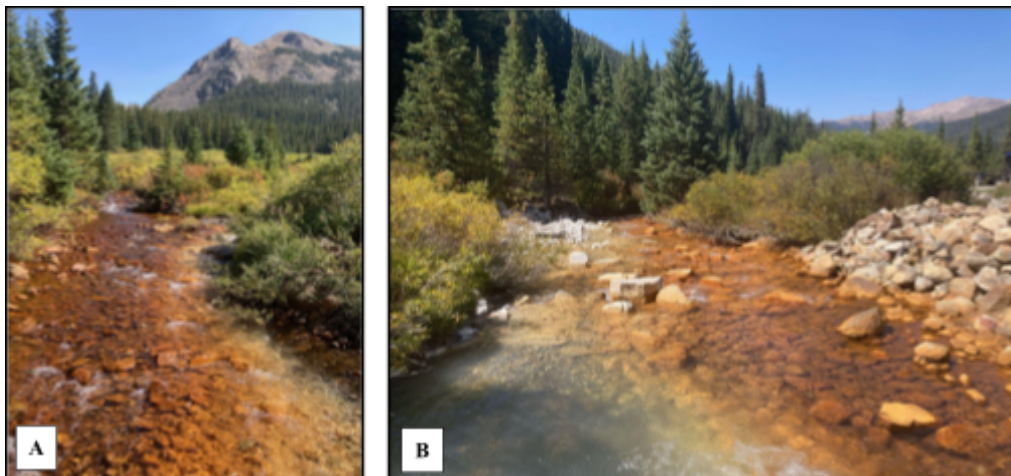


Figure 8. A) Looking upstream of the SN-DC confluence. B) Looking downstream of the SN-DC Confluence.

The Snake River - Deer Creek Confluence (SN-DC) has been studied since the 1950s (Figure 8,9; Theobald et al., 1963). Deer Creek had a pH of 7.4 and Snake River 4.05 in 1957 (Petach, 2022). pH for Snake River in the summer has decreased to less than 3 over time, while Deer Creek has remained above 7 (Rue and McKnight 2021, Todd et al., 2012). Zinc, sulfate, and calcium increased over time. The precipitates at the confluence and found a greater amount of precipitates were in the confluence when the pH was quickly raised when the Snake River confluence with Deer Creek than there were when the pH equilibrated downstream (McKnight et al., 1992; McKnight & Bencala, 1990; Munk et al., 2002). Mineralogical analysis showed that the precipitates were abundant in Zn, Cu, Pb, and Ni ((McKnight et al., 1992; McKnight & Bencala, 1990; Munk et al., 2002)). Rue and McKnight (2021) found cerium depletion and negative cerium anomaly values further downstream in the Snake River where there seems to be a preferential difference in the REEs and the colloidal relationship between Fe and Al.

The DOC variation between Deer Creek and Snake River makes the confluence a unique study area to determine the natural DOC removal processes involving sorption by iron oxides.

DOC concentrations are typically higher than the Snake River by at least a factor of 2 (McKnight et al., 2002). Using a milk truck for transport McKnight et., 2002 injected 23,000 L of fulvic-acid-rich Suwannee River water into the Snake River to determine spatial scale and instream reaction rates of the natural sorbing process. This experiment clearly showed that stream-streambed interactions between abundant iron oxyhydroxides can be a strong control for DOC composition and concentration.

Figure 9. Overview of the SN-DC Confluence.



Little Sayres Gulch, CO

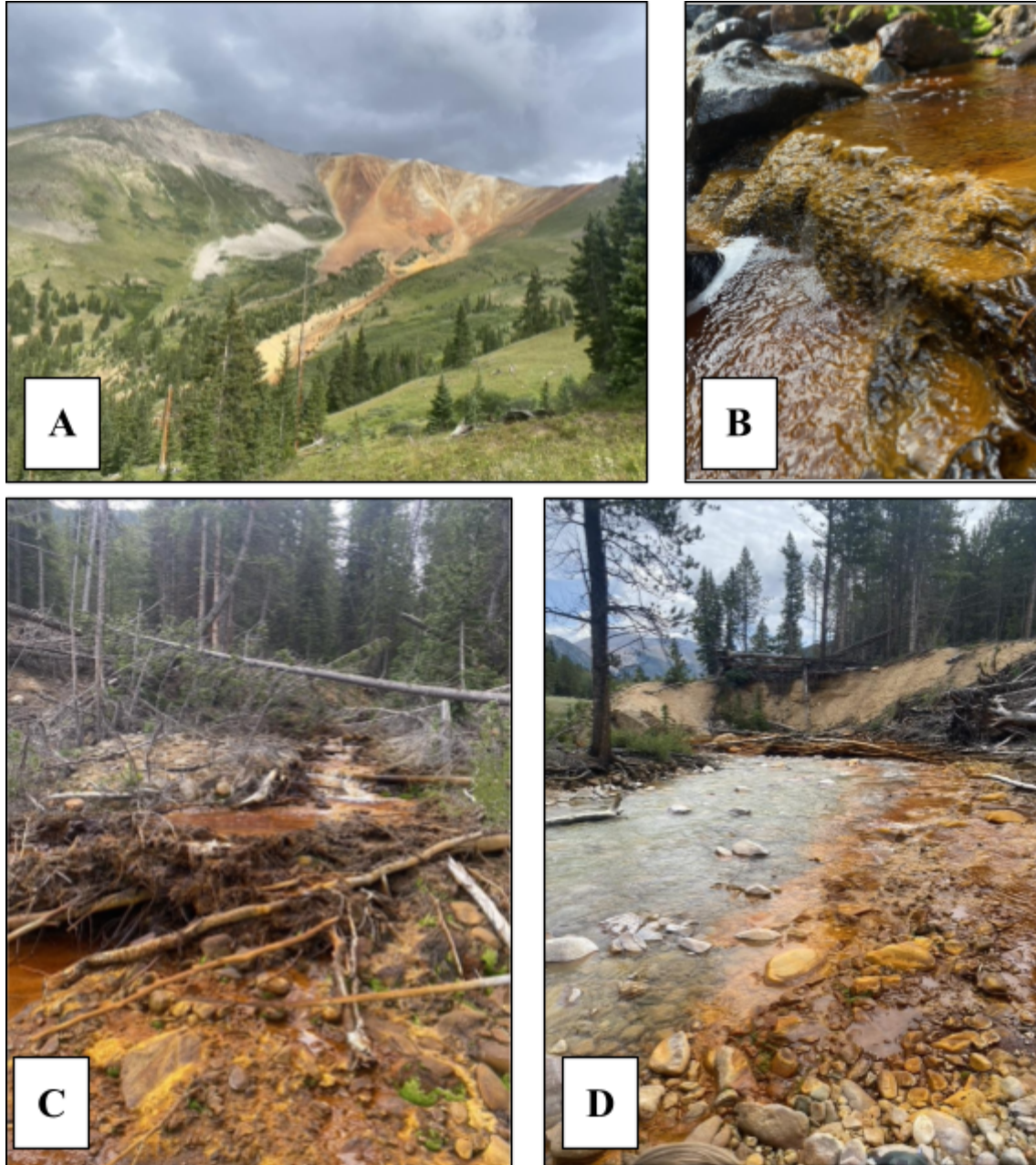


Figure 10. A) Overview of Little Sayres Gulch showing rock differentiation with ARD present. B) Close-up of stream mineral precipitation. C) Photo looking upstream from LS6. D) Confluence of LS on the right with South Creek Lake Fork on the left.

Little Sayres Gulch (LS) (called Sayres Bowl by Bird et. al., 2005) lies southwest of La Plata Peak, CO, and west of Twin Lakes in the Lake Creek watershed. The underlying geology of the watershed is the shallow and intrusive Grizzly Peak Caldera (Bird et al., 2005; Fridrich et al.,

1991). Little Sayres Gulch lies within the East Red Peak area on the far eastern edge of the caldera and is underlay pre-caldera argillic altered rocks aged approximately 40 mya. Magmatic and hydrothermal alteration emplaced rhyolitic dikes and stocks forming Cu-Mo deposits and gold-bearing pyrite veins. Little Sayres Gulch is red and rich in iron (Figure 10 A-C). Upon its confluence with South Fork Lake Creek, there is considerable hydrous oxide precipitation (Figure 10 D). First sampled in 1999 Little Sayres Gulch had a pH of 2.96 (Petach, 2022). Petach sampled in Little Sayres Gulch in 2021 and found that the stream had sulfate concentrations spanning from 600 mg/L to 2600 mg/L from 2000 to 2021. Six sites were sampled along the stream (LS1-LS6) (Figure 11). There were considerable cliffs between LS3 and LS4 making sampling inaccessible. LS7 is after the confluence with South Fork Lake Creek (LF).

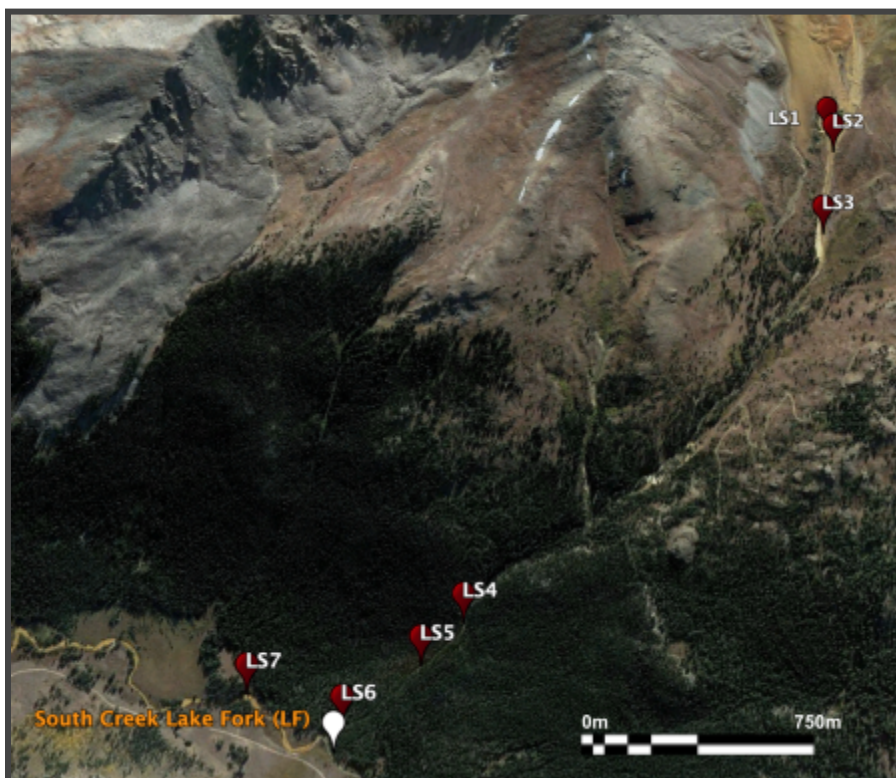


Figure 11. Overview of LS study area indicating sample sites.

Paradise Creek, CO



Figure 12. A) Paradise Creek Confluence with PCT2. B) Downstream before the marsh C) White precipitation of PCT2 next to snow. D) Confluence of Paradise Creek and PCT1.

Paradise Creek, Colorado (PC) is located north of Crested Butte, Colorado in the White River National Forest. Paradise Creek lies in Paradise Basin just below Mount Baldy in the Elk Mountain Range. The Elk Mountain Range formed approximately 34 mya from Oligocene magmas intruding weak areas from the Late Proterozoic orogeny (Payne, n.d.). The main rock type in this area with Tertiary intrusives of andesite and basalt. This location is at an elevation of

11,205 ft and fully above the treeline. Four samples were taken along the main stem (PC1-PC4) (Figure 13). The stream originates in scree and flows through emerging wetlands before making its way below the tree line. The most distinct property of this location is its dominant and apparent aluminum precipitation resulting in a white streambed (Figure 12, A-C). The stream is fed by its initial groundwater and two small tributaries: PCT1 originating in a small lake fed by a small marshy area and PCT2 a stark white stream originating from a seep (Figure 12, C). The Paradise Mine, an abandoned adit, is near the stream to the east, but surface discharge into the sampling area was not observed. Overtime pH has remained consistent (Petach, 2022).



Figure 13. Overview of PC and sampling sites.

California Gulch, CO

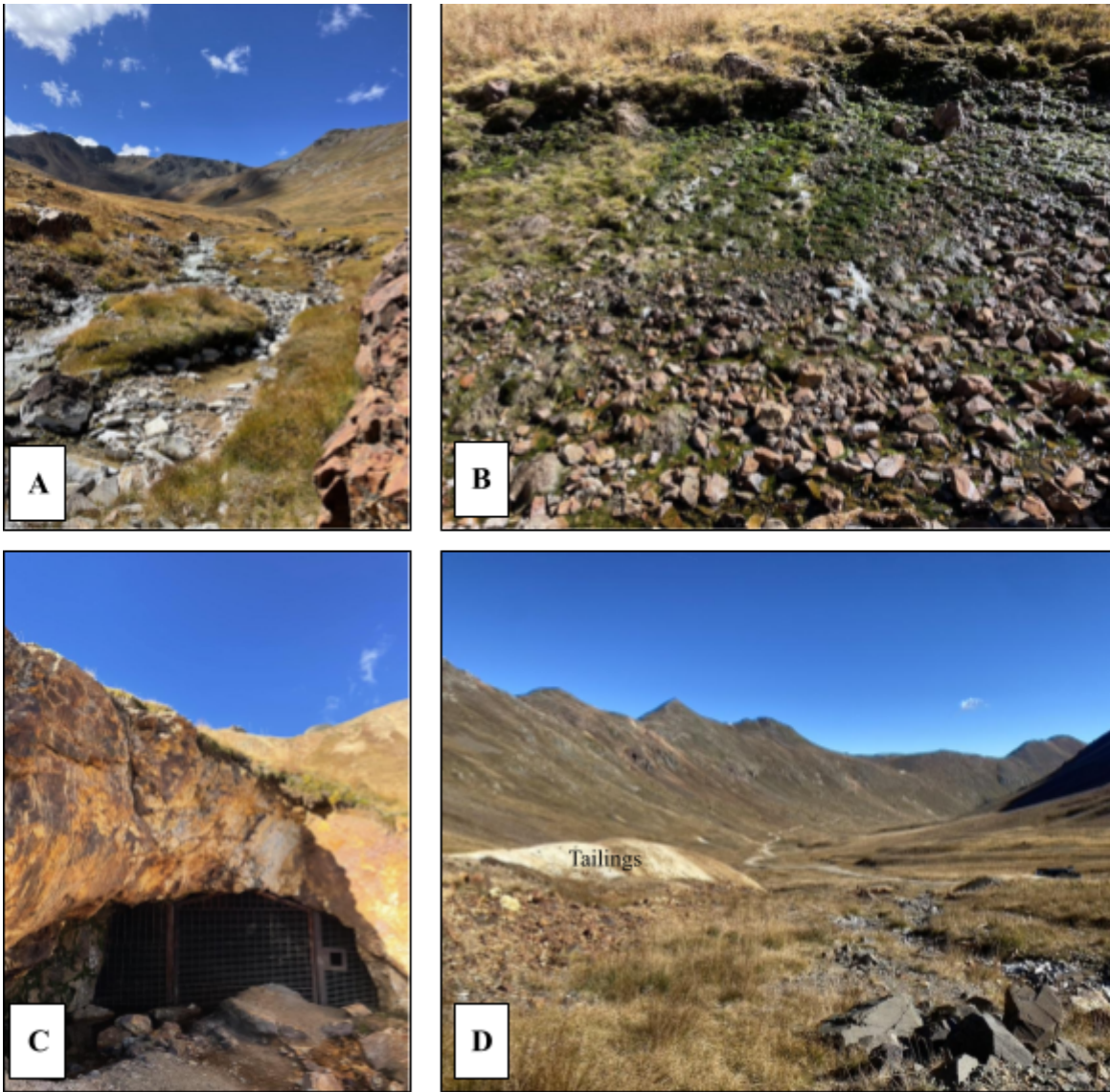


Figure 14. A) Overview of California Gulch looking upstream from CG5. B) Eastern seep (CGS1) containing 1432 ppb total REEs C) Adit/mine with noticeable outflow. D) Looking downstream from CG1 California Gulch with indicated tailing pile from the mine on the left.

California Gulch is along the Alpine Pass trail just east of California Pass near Silverton, CO. California Gulch lies within the Paleogene (23-28 mya) Silverton Caldera (Washington, 2016; Williams & Chronic, 2014). This caldera formed after explosive volcanism and became rich in minerals as the Middle Phase of volcanic and intrusive rocks cool (Williams & Chronic, 2014).

Water circulated through the cooling rock becoming acidic and mobilizing dissolved metals towards the surface creating vein-type deposits surrounded by pyritized rock. The Silverton Caldera has produced more than \$150 million in revenue from mining. This area is known for the Gold King Mine Spill of 2015 where 11,420,000 liters of AMD pulsed into the nearby Animas River making national news (Washington, 2016). This area surrounding California Gulch is influenced by the constant remediation of abandoned and active mines in the area. Along this stream, there are numerous groundwater seeps and one closed mine/extensive adit (CG-Mine)(Figure 15). The location lies above the treeline but flows through a high-altitude marsh before reaching the treeline. This reach was first sampled in 1991 with a pH of 5.09 (Petach, 2022). Petach (2022), found the Zn and sulfate concentrations had increased over time. Eight samples of the main stem were taken (CG1-CG8) (Figure 15). Two major seeps were sampled (CGS1- Eastern Seep and CGS2- Western Seep) (Figure 15).

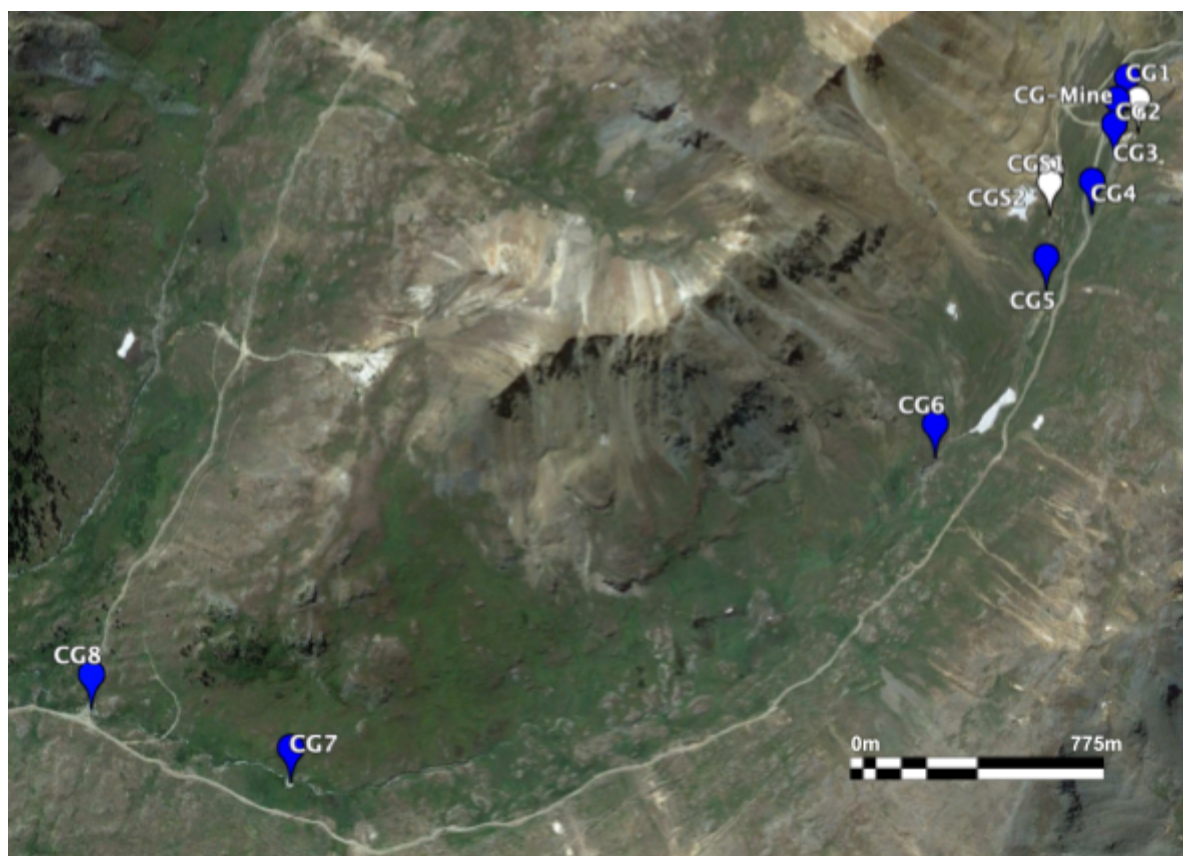


Figure 15. Overview of California Gulch and sampling sites.

2.2 Field measurements

During the synoptic sampling UTM coordinates were taken at each site. Conductivity and pH were recorded with a Hanna HI 9033 Multi-range conductivity meter and Hanna HI 9023 microcomputer pH Meter. Water samples were collected in 250 ml HDPE trace-metal grade 5% M HNO_3^- acid washed bottles. These bottles and their caps were rinsed three times with stream water. The 250-mL sample was then filtered through a $0.45 \mu\text{m}$ 47 mm Nucleopore membrane to filter out larger particles using a hand pump and plastic filtration unit and placed into 2 labeled bottles: 1) 125-mL for REE and cation analysis with 3.75 ml of 0.1 M HNO_3^- acid preservation and 2) 60-mL for anion analysis without acid preservation. Dissolved organic carbon (DOC) samples were collected in 250-mL glass amber bottles that had been combusted for 4 hrs at

450°C. These bottles and their caps were also rinsed three times with stream water. Filtered through 0.45 μm pre-combusted at 450°C for two hours (USGS) GF/C membranes and filtered into 2 clean and combusted 120-mL amber glass bottles. In the first bottle, 0.5 ml of 1 M HCl into the first 120 ml to preserve the sample for DOC analysis. The second bottle for fluorescence characterization did not receive HCl preservation. Flocculant was collected by scrubbing a streambed rock with flocculant present in a small bin with stream water. Flocculant and water were collected in 500 mL HDPE acid-washed bottles. All samples were kept on ice and refrigerated at 4°C once returned to the lab. Surface area measurements to normalize the amount of flocculant per mm^2 were done by foil wrap analysis (Dudley et al., 2001).

2.3 Lab Analysis

Each water sample was analyzed for the cation concentrations. All REEs (La, Ce, Pr, Nd, Pm, Sm, Eu, Gd, Tb, Dy, Ho, Er, Tm, Lu, Y), major cations, and trace metals (Al, Cd, Cu, Co, Mn, Ni, Pb, Zn) were determined by the INSTAAR Trace Metal Lab at CU Boulder by Dr. Thomas Machitto on a Thermo Finnigan Element 2 ICP-MS. Highly concentrated samples were diluted 1:2 with 4% nitric acid to then calculated for total concentration.

Fe and charge balance cations (K, Mg, Ca, Na) were run on a Perkin Elmer 200 Flame Atomic Absorption Spectrometer (FAAS) with an acetylene flame. Fe, K, Mg, Ca, Na were spiked with 1 mL Lanthanum Chloride as a releasing agent (*METHOD 7000B FLAME ATOMIC ABSORPTION SPECTROPHOTOMETRY*, 2007). Highly concentrated Fe samples were diluted 1:100 to stay within detectable concentrations.

Anion analysis was done with Ion Chromatographer (IC) Dionex ICS-2000 with an AS40 autosampler with the help of Post Doc Marisa Repasch. To avoid metal precipitation in the IC

from the addition of KOH eluent because of the low pH of the samples each sample was pretreated with varying amounts and concentrations of NaOH to bring the sample up to a pH of 6-7.5 and precipitate Fe and Al prior to analysis. After pretreatment, samples were centrifuged at 300 rpm for 10 minutes to concentrate precipitates, and an aliquot of 4 mL was taken for analysis immediately after centrifuge.

Dissolved Organic Carbon was measured by Shimadzu TOC-VCSH Analyzer WITH ASI-L autosampler in the Environmental Engineering Laboratories at SEEC. Samples with a conductivity measurement of greater than $7000\mu\text{S}/\text{cm}$ were diluted 1:10 with ultra-pure water to ensure machine safety. Fluorescence was measured by a 2-D fluorescence scan on a FluoroMax-3 with DataMax software with a single excitation wavelength at 370 nm to obtain the emission spectra. To account for Raman scattering as a result of non-elastic, scatter Raman correction was done by putting the fluorescence in terms of Raman Units (R.U) (Lawaetz & Stedmon, 2009).

Flocculant collected was left to settle to allow excess water to be siphoned using an aspirator. The flocculant was then transferred to acid-washed 50-mL Falcon centrifuge tubes and centrifuged at 5000 rpm for 10 minutes. Excess water was siphoned for a second time before sediment was transferred to aluminum trays and dried overnight in an oven at 70°C . For metal analysis, ~25 mg of dried flocculant was added to 50-mL acid-washed Falcon centrifuge tubes. Mass was recorded for each sample prior to and after dilution for dilution and mass calculations. 1-mL of concentrated optimum nitric acid was added and samples were heated on a hot plate in water for a minimum of 3.5 hours and left to sit in acid for 3 days. Samples were diluted to 50 mL and centrifuged to concentrate undissolved silica-based sediment and an aliquot of the solution was taken for analysis. For mass percent of total carbon (organic and inorganic) and

nitrogen, dry flocculant samples were weighed and combusted with a Costech ECS 4010 elemental combustion system (elemental analyzer) by Jimmy McCutchan and Erin Jaynes in the SEEL Limnology Lab.

2.4 Theory

Fluorescence

Fluorescence is useful for determining the source and chemical composition of dissolved organic matter (DOM). Various indices use the emission at specific excitations to make these determinations.

Eq. 1. Raman Correction (Lawaetz & Stedmon, 2009)

$$F_{\lambda_{ex}, \lambda_{em}} (R.U.) = \frac{I_{\lambda_{ex}, \lambda_{em}} (A.U.)}{A_{rp}}$$

The correction for the Raman scattering of water is necessary to obtain an accurate measurement of fluorescence. Wavelength is normalized to A_{rp} . A_{rp} is the calculated integral of the Raman peak as calculated with the DataMax software. Where R.U. is Raman Units, and FI is the fluorescence corrected for the blank.

Eq. 2. Fluorescence Index (McKnight et al., 2001)

$$FI = \frac{F_{\lambda 470} (R.U.)}{F_{\lambda 520} (R.U.)}$$

The fluorescence index (FI) coined by McKnight et. al (2001) used emitted wavelengths at 470 nm and 520 nm to determine the source of DOM. Where FI of 1.7-2.0 is microbially derived

1.3-1.4 is soil and plant litter driven. FI is calculated by dividing the Raman corrected units at 470 nm and 520 nm.

Cerium Anomaly

Cerium (III) is unique because it is the only REE that readily oxidizes to insoluble (IV) (Verplanck et al., 2004). Ce concentration can be disproportionately low compared to other REEs (Moffat, 1994). Using neighboring atomic elements La and Pr, we can calculate a more accurate representation of Ce. The ratio between Ce in a sample and standardized concentrations of La and Pr can indicate new redox conditions influencing Ce concentrations relative to the concentrations of adjacent REEs. This calculation is designated the cerium anomaly (Ce*). More positive values of Ce* indicate reducing conditions and a higher concentration of dissolved Ce. More negative values indicate oxidizing conditions and lower dissolved concentrations of Ce. Normalization of Ce to a standard indicates relative enrichment or depletion. Common practice is to normalize to the Post-Archean Australian Shales (PAAS) or North American Shale Composite (NASC), however, within this study, it seems more appropriate to standardize water samples to the Paradise Portal standard obtained from the Paradise portal in the upper Animas River basin, Colorado (Verplanck et al., 1999) (Table 5, 6). To compare the standardization standardizing each location's Ce to itself by choosing the site within the location with the highest total REEs.

Eq. 3. Normalization of REE in the sample to standard

$$\text{Standardized Sample (Ce, Pr, La)} = \frac{\text{Sample element concentration}}{\text{Standardized element concentration}}$$

Eq. 4. Cerium Anomaly (Ce) Calculation*

$$Ce^*_{Standard} = \frac{(2 * Ce_{standardized\ sample})}{(La_{standardized\ sample} + Pr_{Standardized\ Sample})}$$

Redfield Ratio

The Redfield Ratio is a globally static atomic ratio used to understand the biogeochemical relationships between organisms and the environment (Redfield, 1958). To calculate the ratio from percent carbon and percent nitrogen measured per microgram in streambed flocculant samples unit conversion was used to convert to mols of carbon and nitrogen. The ratio was then calculated by dividing carbon mols by nitrogen mols. Microorganisms have a ratio of approximately 8, humus approximately 11, and terrestrial riverine approximately 14 (Prahl et al., 1994; Schwyter & Vaughan, 2021).

Two Sample T-test

A two-sample T-test was performed in R Studio to determine whether there is a significant difference between the amount of total REEs in flocculant samples with high aluminum compared to those with high iron concentrations. The null hypothesis was that there was no difference between the amount of REEs in the aluminum-rich flocculant vs. iron rich-flocculant.

3.0 RESULTS

3.1 Iron Hill

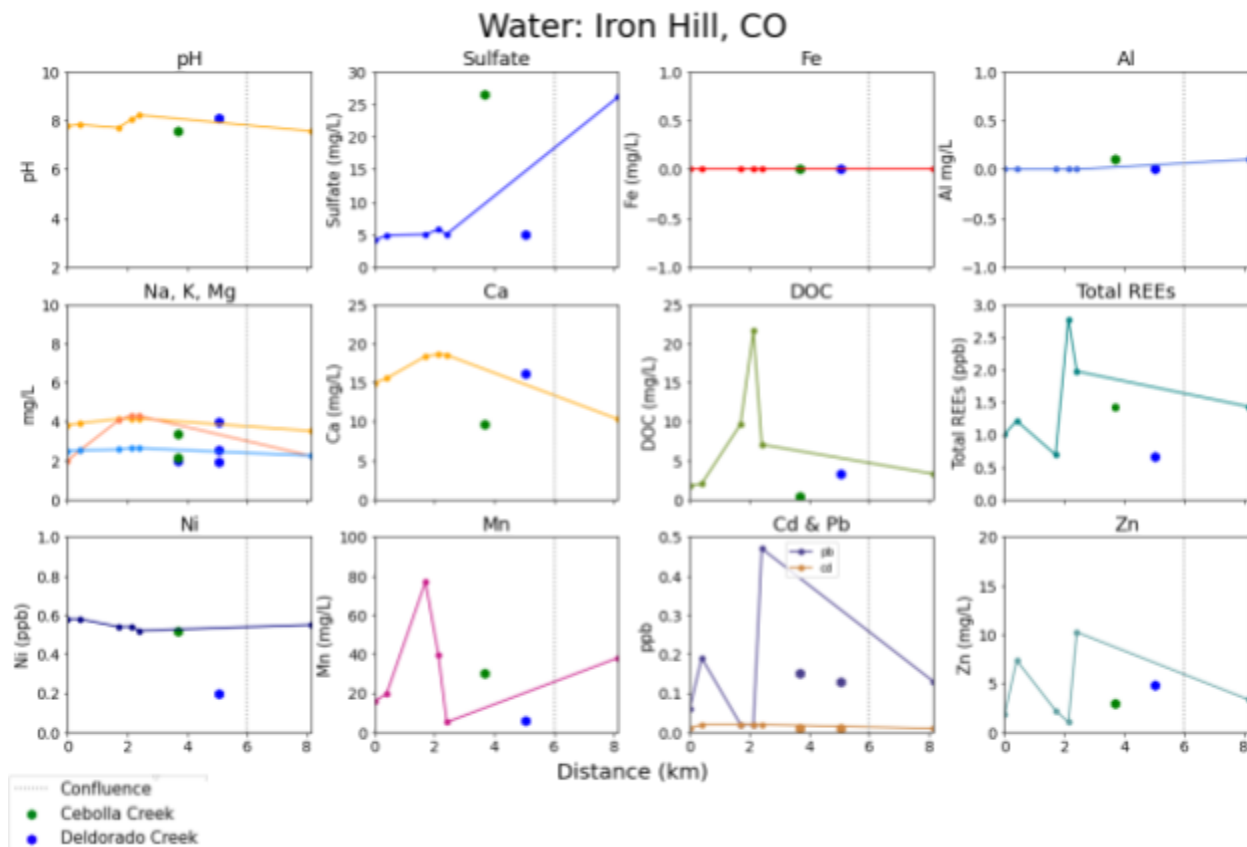


Figure. 16 Water chemistry (pH and relevant dissolved concentrations) of Iron Hill. Distance refers to the downstream distance of the Beaver Creek reach. The gray line is the confluence of all sample sites.

This location was chosen because of its known high concentrations of REEs in the carbonatite rock, and its lower elevation below the tree line. The water chemistry analysis shows minimal metal mobilization (Figure 16). The pH of this location remained above 7. The greatest increase of sulfate occurred after the confluence of Cebolla and Deldorado Creek from 5 mg/L to 27 mg/L. Fe and Al concentrations remained below detection within the creek and below the confluence. Ca concentrations increased as Beaver Creek became within closer proximity to Iron Hill. DOC concentrations were elevated in BC3-BC4. This was also the trend for total REEs,

which increased from ~1.0 to almost 3.0 ppb. Cd and Pb concentrations remained stable at low concentrations, <0.05 ppb and <0.5 ppb, respectively, throughout the sampling area.

3.2 Tributary 2095

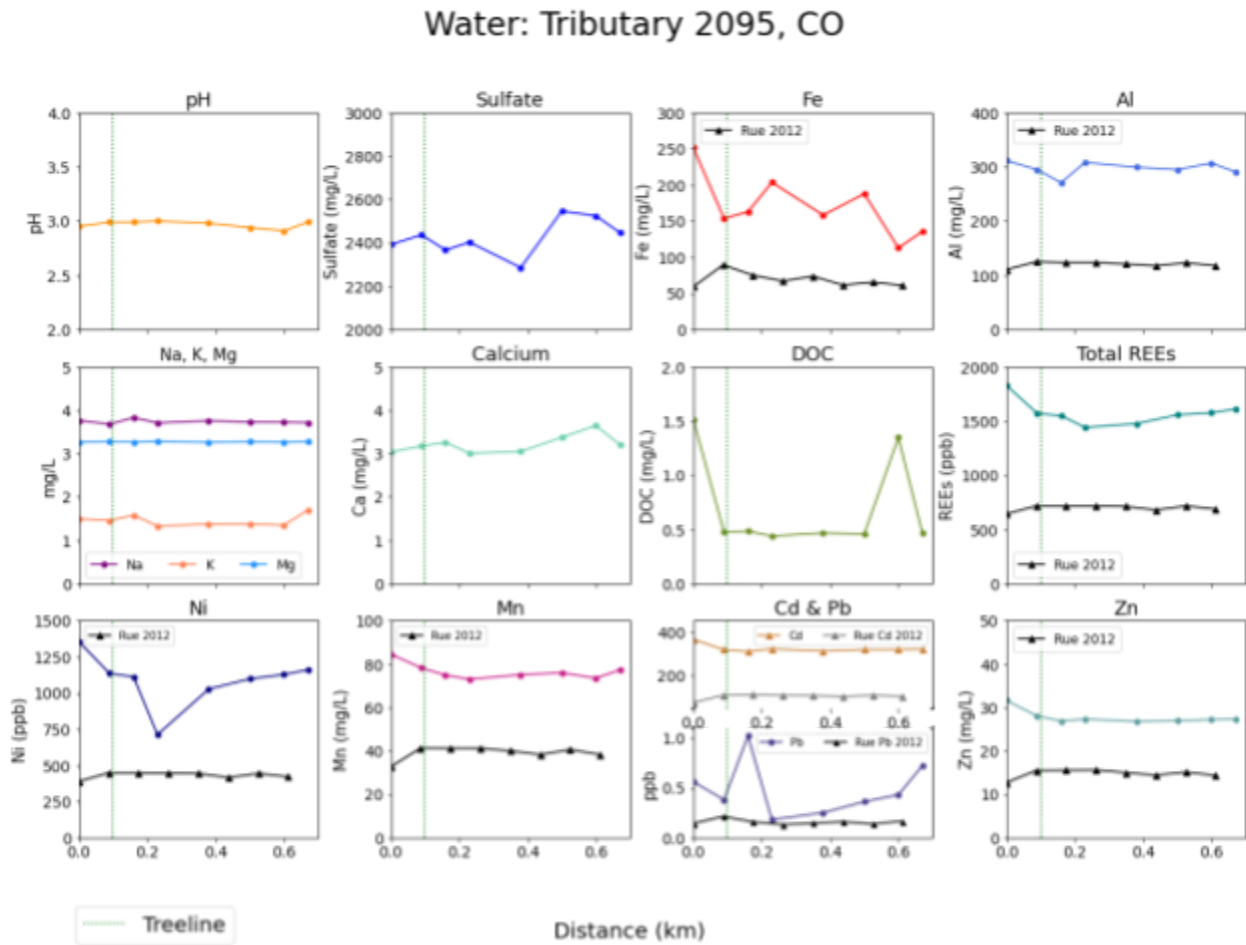


Figure 17. Water chemistry (pH and relevant dissolved concentrations) of tributary 2095 of the Snake River. The green dotted line represents the treeline.

The water chemistry of tributary 2095 showed a consistent pH of 3 (Figure 17). Sulfate concentrations began at ~2400 mg/L, then decreased and followed by an increase for the lower sample sites. The dissolved Fe concentrations were highest at 250 mg/L at the most upstream site and decreased at treeline and continued to decrease erratically until concentrations were ~120 mg/L at the lowest sites. This overall decrease indicates the potential for precipitation of hydrous

metal oxides. The concentrations of Al, Na, K, Mg, and Ca remained generally constant throughout the reach. DOC concentrations started relatively low from 0.5 to 1.5 mg/L, dropped and then doubled at site 2095-7. The concentration of total REES was highest at the upstream site at ~1900 ppb, decreased at the tree line, and it gradually increased downstream. The concentrations of Mn, Cd, and Zn, followed a similar pattern as the upstream REE peak. The most notable result is the differences in metal concentrations between the Rue 2012 samples and the 2022 samples. There is a 3 fold increase in concentrations for Fe, Al, Ni, Mn, total REEs, and Zn.

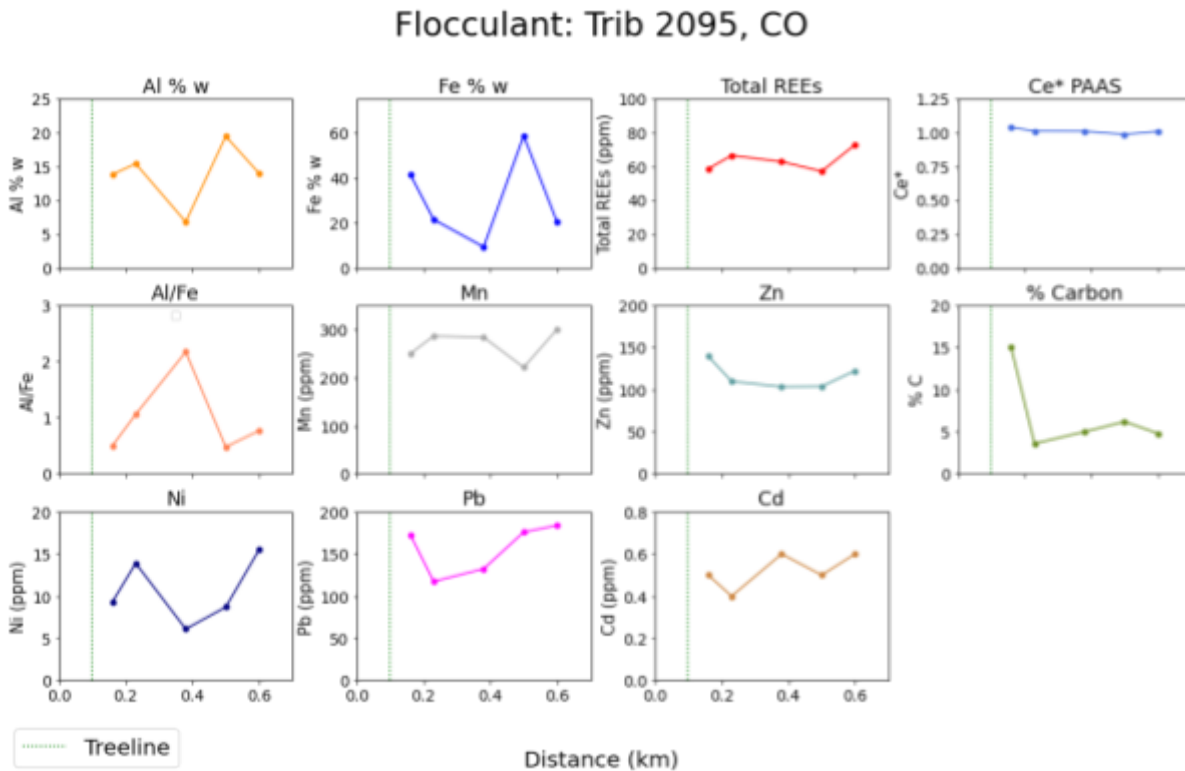


Figure 18. Flocculant chemistry of tributary 2095. The green dotted line represents the treeline.

Flocculant chemistry showed a low concentration of Al and a high concentration of Fe (Figure 18). This result indicates that there was hydrous iron oxide precipitation, which is consistent to

the decreased Fe concentrations found in the water chemistry. Ce* remained around 1.0 suggesting the stream is mostly reducing in this context. Al/Fe varied but minimally within the overall low ratio. Mn content remained above 200 ppm throughout the reach of the stream. The carbon content dropped in the flocculant from 8% to between 2-3% going downstream. The content of total REEs were consistent at ~60 ppm. The Pb content was elevated at ~120-170 ppm, exceeding the total REE content, whereas the Ni and Cd concentrations were much lower than Pb and total REEs

3.3 Snake River - Deer Creek Confluence

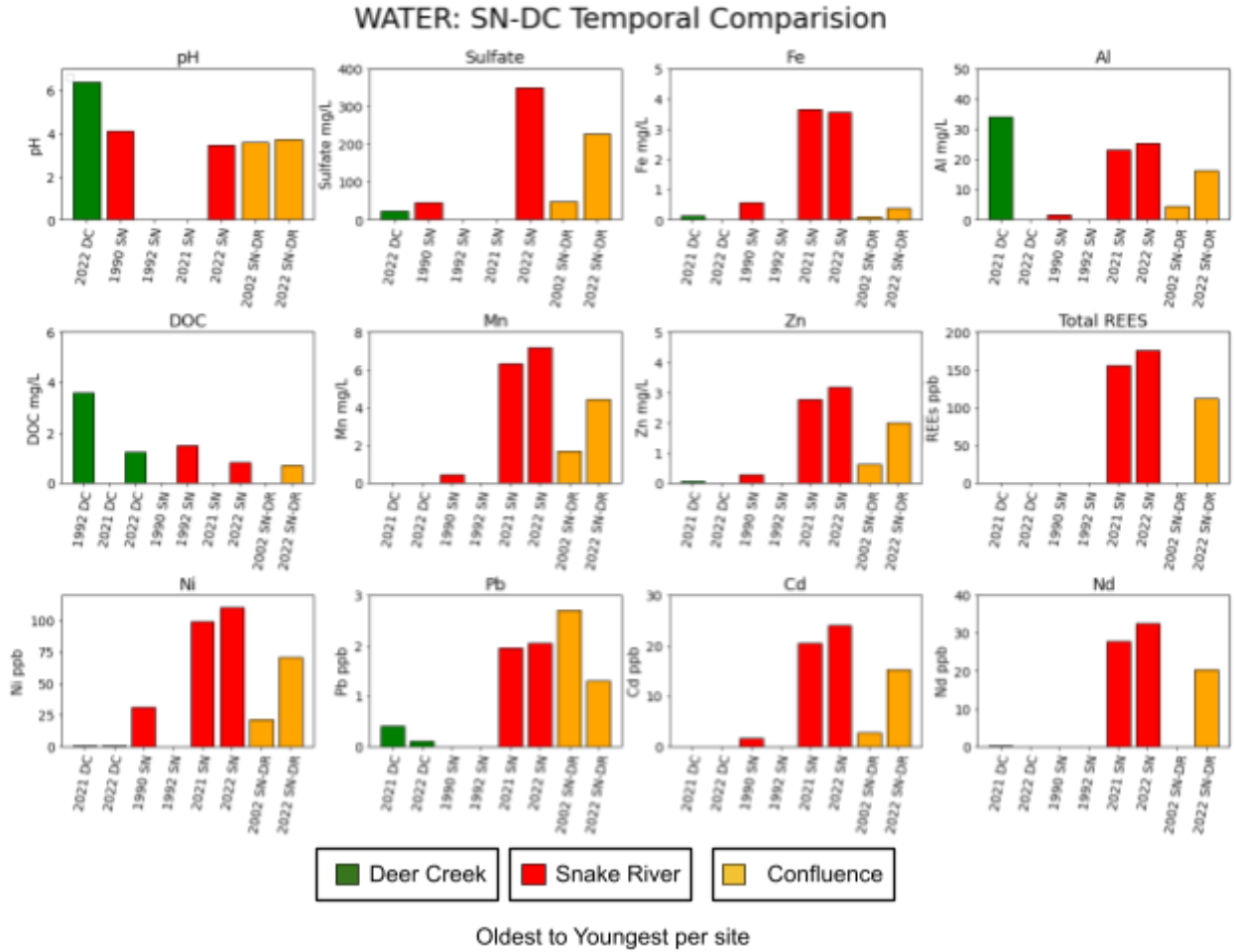
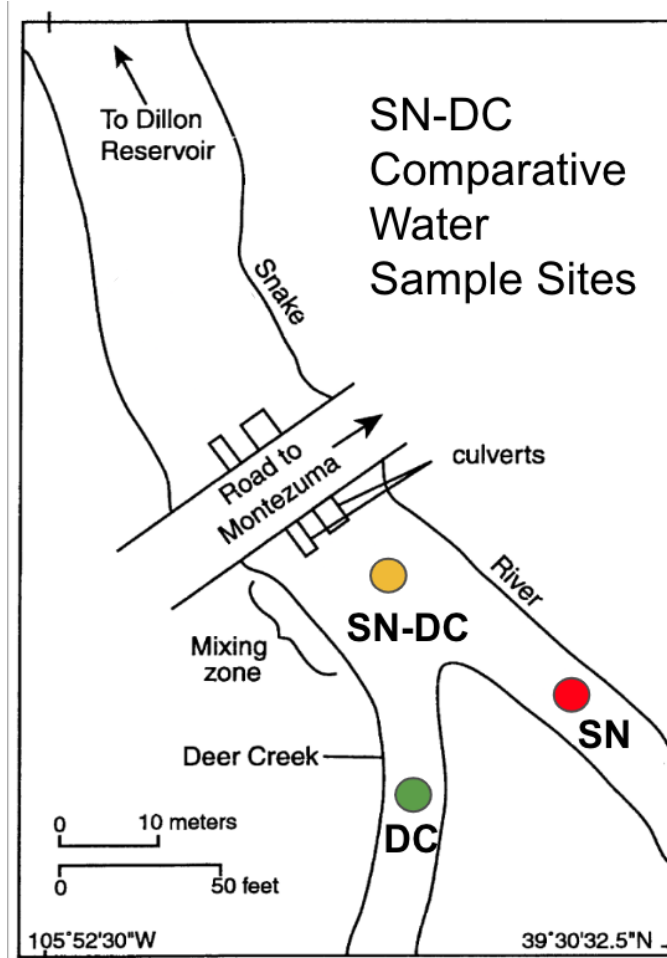


Figure 19. (above) Snake River - Deer Creek temporal comparative available data. 1990, 1992 values from McKnight et., (1990 & 1992); 2002 data from Munk et. al. (2002); 2021 from Petach (2022).

Year	Sample & Reference	pH	DOC	Fe	Al	SO4-	Mn	Zn	Ni	Cd	Pb	Total REEs
			ppm					ppb				
1992 DC	DC5, 1992, Mcknight	nm	3.6	nm	nm	nm	nm	nm	nm	nm	nm	nm
2021 DC	DC, Petach, 2021	nm	nm	0.1305	34	nm	0.02305	0.075	0.3	0.0335	0.4	0.5915
2022 DC	DC, Brooks, 2022	6.36	1.226	0.008	0	24.05	0.019	0.018	0.8	0.03	0.1	0.25
1990 SN	SN2, 1990, McKnight	4.13	nm	0.57	1.75	46.4	0.44	0.29	31	1.6	nm	nm
1992 SN	SN2, 1992, McKnight	nm	1.5	nm	nm	nm	nm	nm	nm	nm	nm	nm
2021 SN	SN, Petach, 2021	nm	nm	3.645	23.05	nm	6.32	2.765	98.85	20.5	1.955	155.468
2022 SN	SN, 2022, Brooks	3.47	0.8295	3.57	25.4	348.84	7.185	3.188	110.09	23.98	2.05	175.7
2002 SN-DC	1W, Munk, 2002	3.6	nm	0.12	4.38	49.2	1.7	0.614	21.3	2.81	2.71	nm
2022 SN-DC	SN-DC, Brooks, 2022	3.71	0.718	0.396	16.3	227.5	4.436	1.981	70.9	15.29	1.3	111.6

Table 1. Values used for SN-DC comparison with associated references. Not measured (nm).

Figure 20. (below) An overview map of the SN-DC water sampling sites, adapted from Munk et al., 2005.



The temporal comparison of water measurements since 1990 indicates changes in concentrations over the last 32 years. (Figure 19, 20). Deer Creek showed a decrease for similar summer conditions in DOC concentration from ~4 mg/L in 1992 to ~ 1 mg/L in 2022. Snake River had decreased in pH and DOC, but had large increases in all metals since 1990. The most notable increase was in the Snake River where sulfate increased from ~40 to 350 mg/L (1990-2022), Al from ~2 to 20 mg/L (1990-2022), and Zn from ~0.5 to 3.1 mg/L (1990-2022). Temporally most water chemistry concentrations had increased.

SN-DC Confluence Temporal Flocculant Comparision

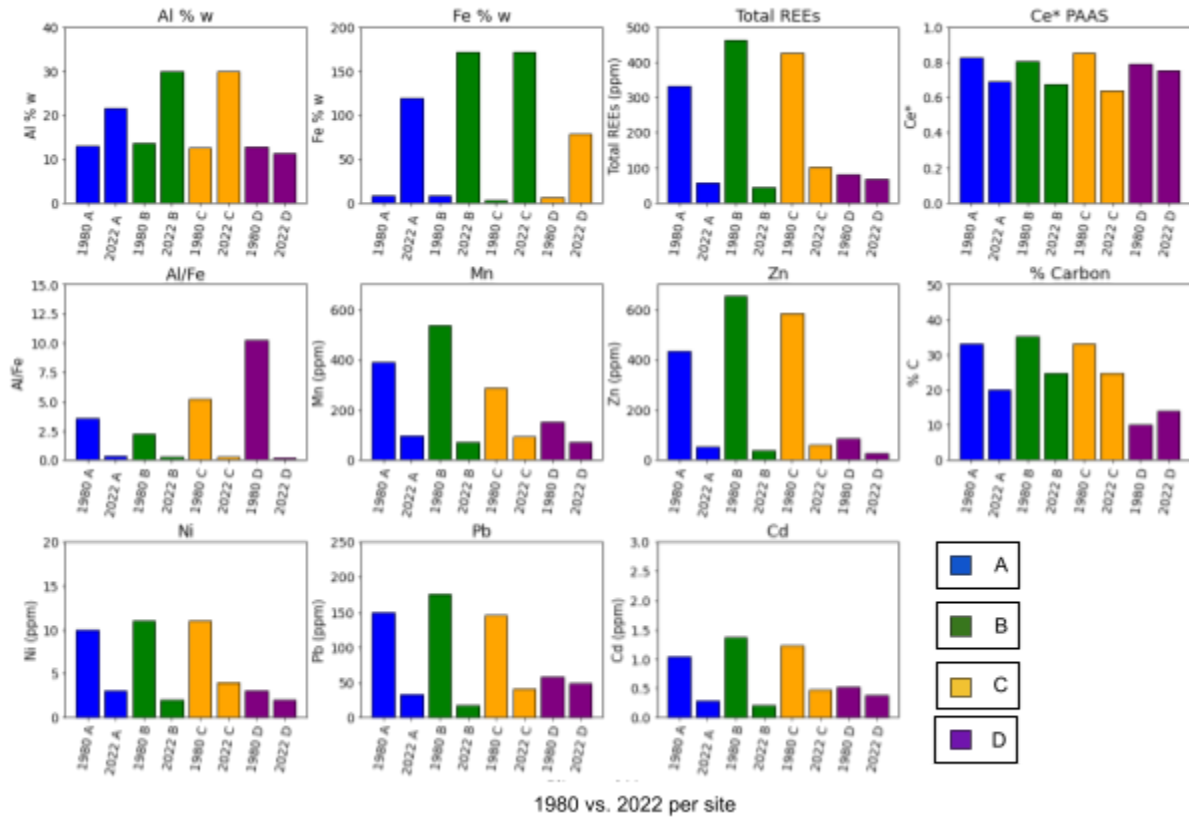
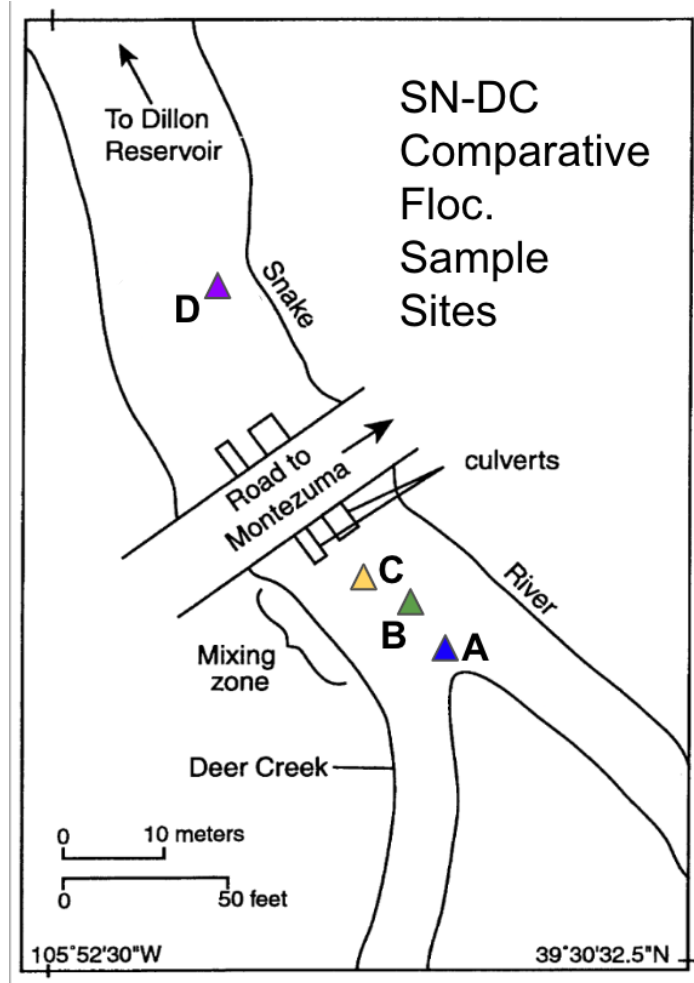


Figure 21. (above) Flocculant data comparison between 1980 and 2022.

Figure 22. (below) Overview of flocculant sample sites A-D. Adapted from Munk et al., 2005.



Comparison among flocculant samples from 1980 and 2022 suggested a shift from a composition that was Al dominant to Fe dominant. Total REEs, Mn, Zn, Ni, Pb, and Cd concentrations within the flocculant decreased in 42 years. Sites A-C had similar trends and concentrations within the same sampling year displaying a consistency within the sample for the time. Site D is further downstream and is more representative of post-mixing zone precipitation. Total REEs, Mn, Zn, carbon contents, Ni, Pb and Cd concentrations were lower regardless of the year at this site. Site D had the highest concentration of percent Fe in 2022.

3.4 Little Sayres Gulch

Water: Little Sayres Gulch, CO

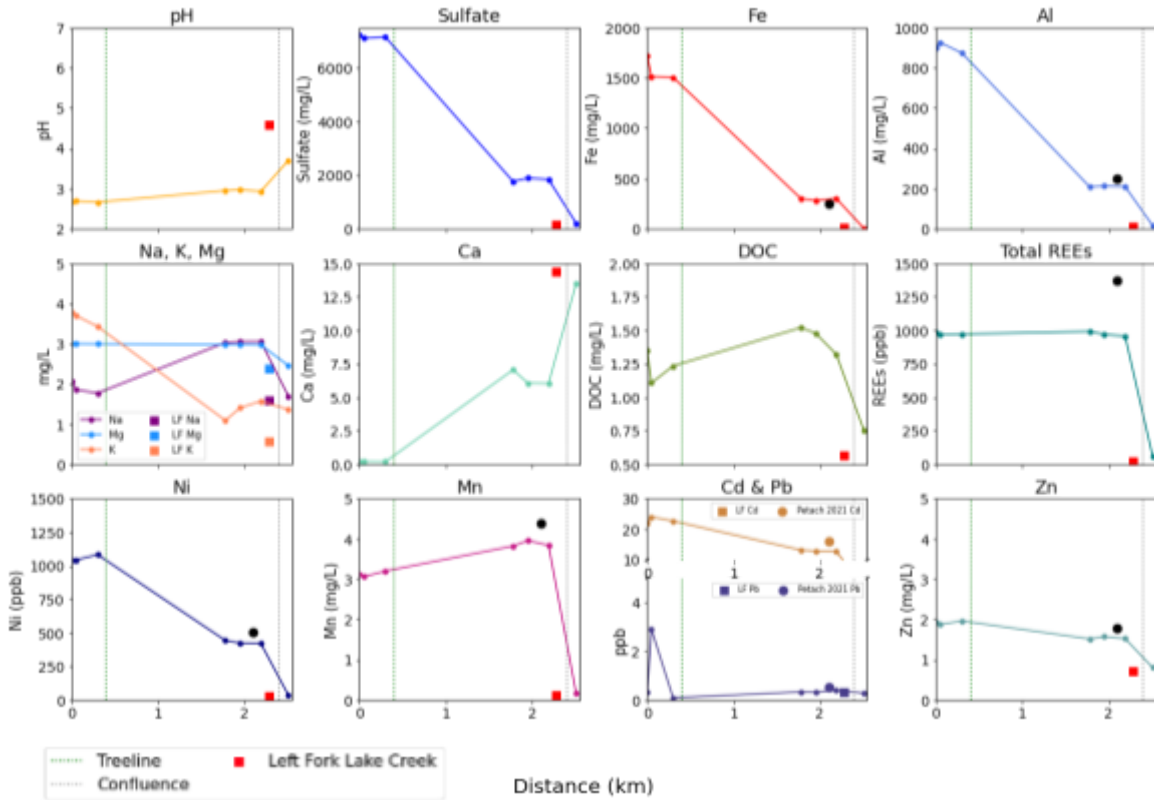


Figure 23. Water chemistry (pH and relevant dissolved concentrations) of Little Sayres Gulch. The green dotted line indicates the treeline and the grey dotted line indicates the confluence.

The pH of Little Sayres Gulch remained below 2.75 until the confluence with the more basic Left Fork Lake Creek (LF) (Figure 23). Sulfate started at 7200 mg/L and decreased to less than 2000 mg/L below the treeline. Fe concentrations began at 1750 mg/L and greatly decreased below treeline to ~400 mg/L. Al and Ni concentrations followed similar trends. Ca increased downstream. Inversely, DOC increased slightly from 1.2 to 1.5 mg/L and then decreased to 0.7 mg/L. REEs exhibited stable concentrations within the stream until after the confluence with LF, when they dropped quickly out of solution.

Flocculant: Little Sayres Gulch, CO

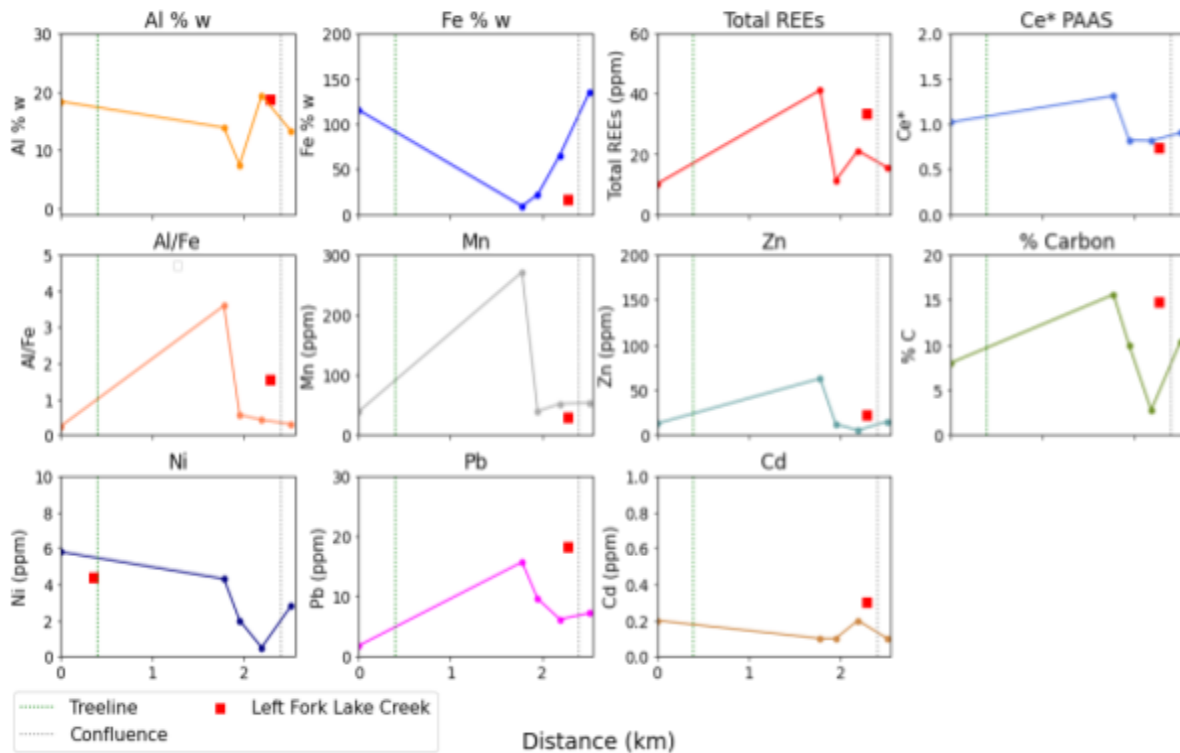


Figure 24. Flocculant chemistry of Little Sayres Gulch. The green dotted line indicates the treeline and the gray dotted line indicates the confluence with Left Fork Lake Creek.

Little Sayres Gulch flocculant was much higher in Fe than Al (Figure 24). Total REEs increased until the first sampling site (LS4) in the sub-alpine forest, where the concentration quickly decreased by more than half. Organic carbon content increased 2-fold from the beginning of the stream to the first point below the treeline, where it decreased after the confluence with Left Fork Lake Creek. Ni concentration dropped below tree line.

3.5 Paradise Creek

Water: Paradise Creek, CO

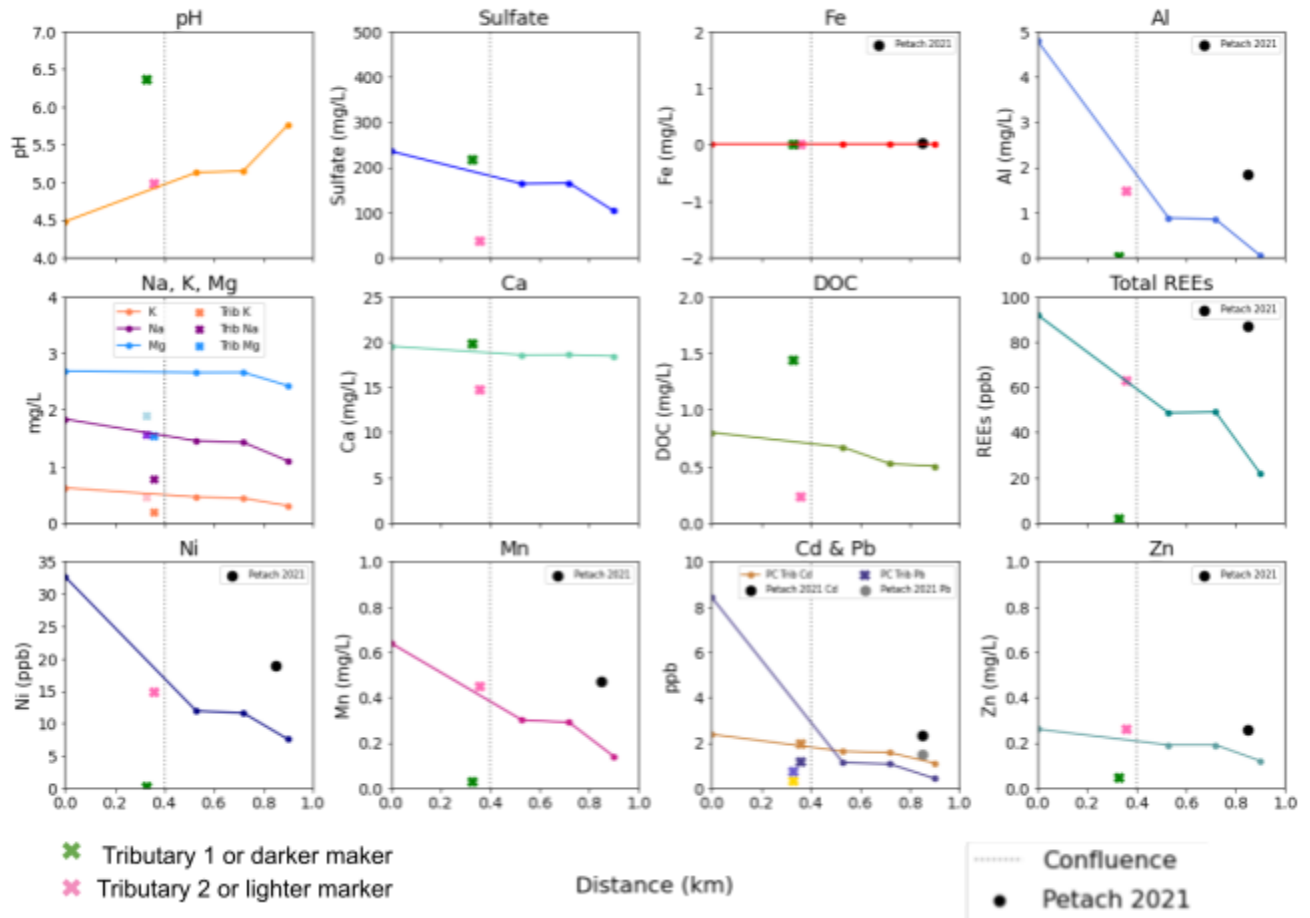


Figure 25. Water chemistry of Paradise Creek. The gray dotted line represents the confluence.

The pH of Paradise Creek increased after the confluence of both tributaries and continued to increase as it flowed through the marsh (Figure 25). Sulfate concentrations started around 250 mg/L and decreased to 100 mg/L along the sample reach. Fe concentrations were negligible. Al decreased from ~5 mg/L to below detection in sample sites within the marsh area below the confluences. The concentrations of Na, K, Mg, Ca, Zn, and DOC gradually decreased. The trace metals such as Ni, Mn, Cd, and Pb all decreased inversely with the rising pH.

Flocculant: Paradise Creek, CO

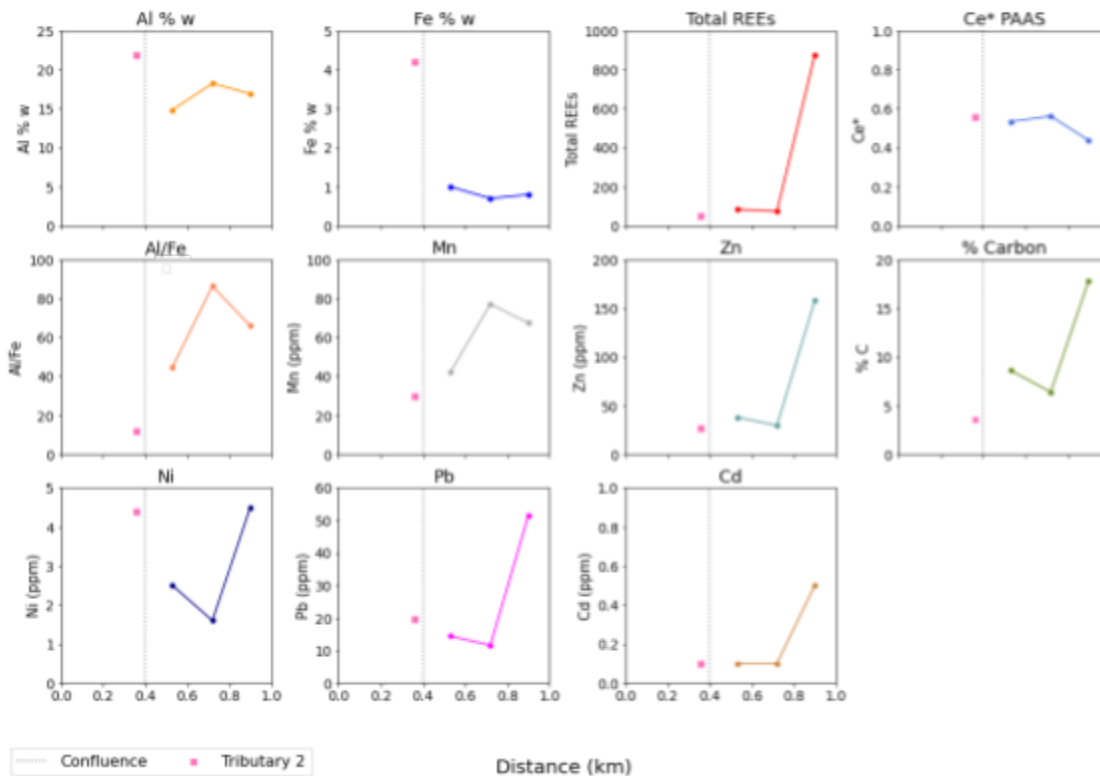


Figure 26. Paradise Creek flocculant chemistry. The gray dotted line indicates the confluence.

Flocculant from Paradise Creek had an Al content of ~15-20% and was dominant in Al (Figure 26). REE concentrations in the flocculant were extremely high at the end of the stream sampling site with totals of just under 1000 ppm corresponding to the highest flocculant concentration of REEs in this study. The Ce* decreases in this same site. Most all trace metals increased in the flocculant when progressing downstream. This finding supports the observed decrease of trace metals in the water chemistry.

3.6 California Gulch

Water: California Gulch, CO

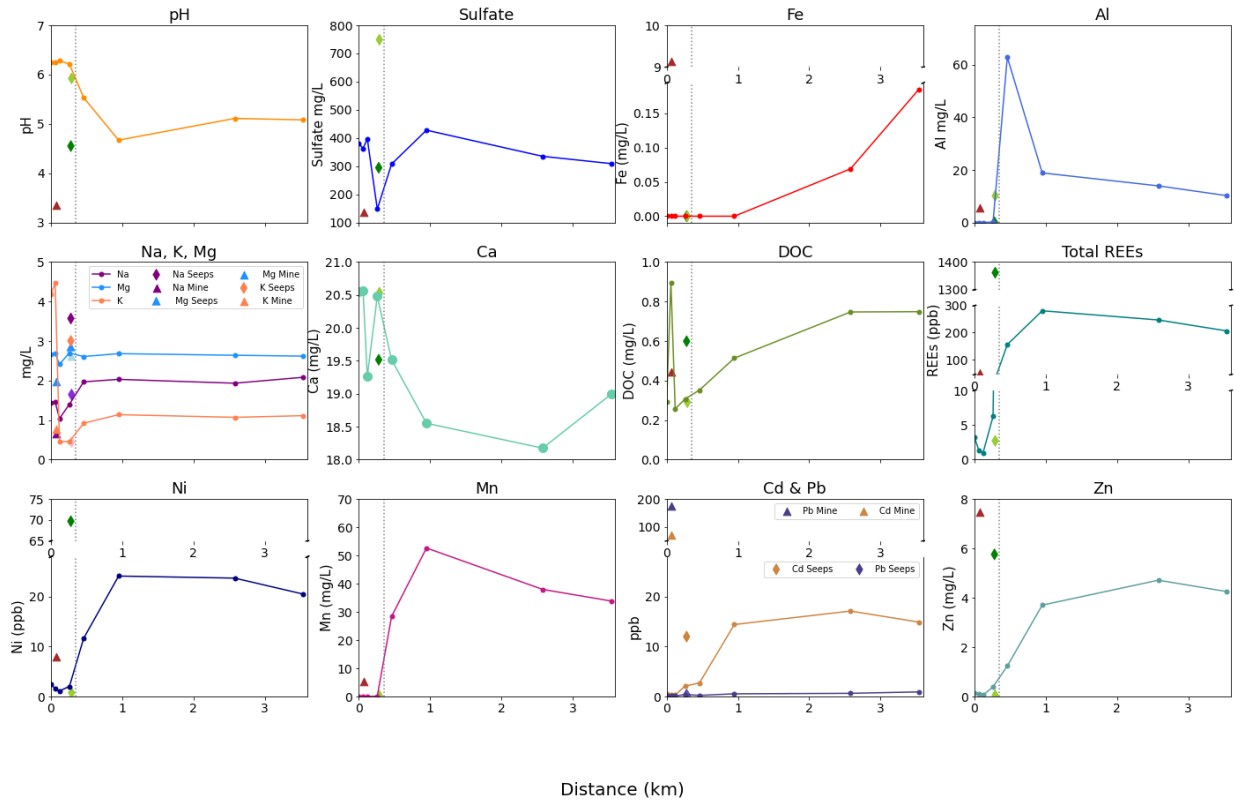


Figure 27. California Gulch water chemistry (pH and relevant dissolved concentrations). The gray dotted line represents the confluence of CG-Mine, CGS1, and CGS2 with the main stem of California Gulch

The complexity of this location can be seen in the synoptic sampling results. Sulfate, Al, Ca, total REEs, Ni, Mn, Cd, and Zn all increased after the confluence with both seep and mine inputs, which had the highest concentrations (Figure 27). CGS1 yielded high concentrations of total REEs at over 1400 mg/L and Ni ~70 mg/L. CG-Mine had the highest measured concentration of Fe compared to other sites in California Gulch. DOC concentrations were low, less than 1 mg/L, and increased during reaches within the marshy fen as metal concentrations stabilized or decreased.

Flocculant: California Gulch, CO

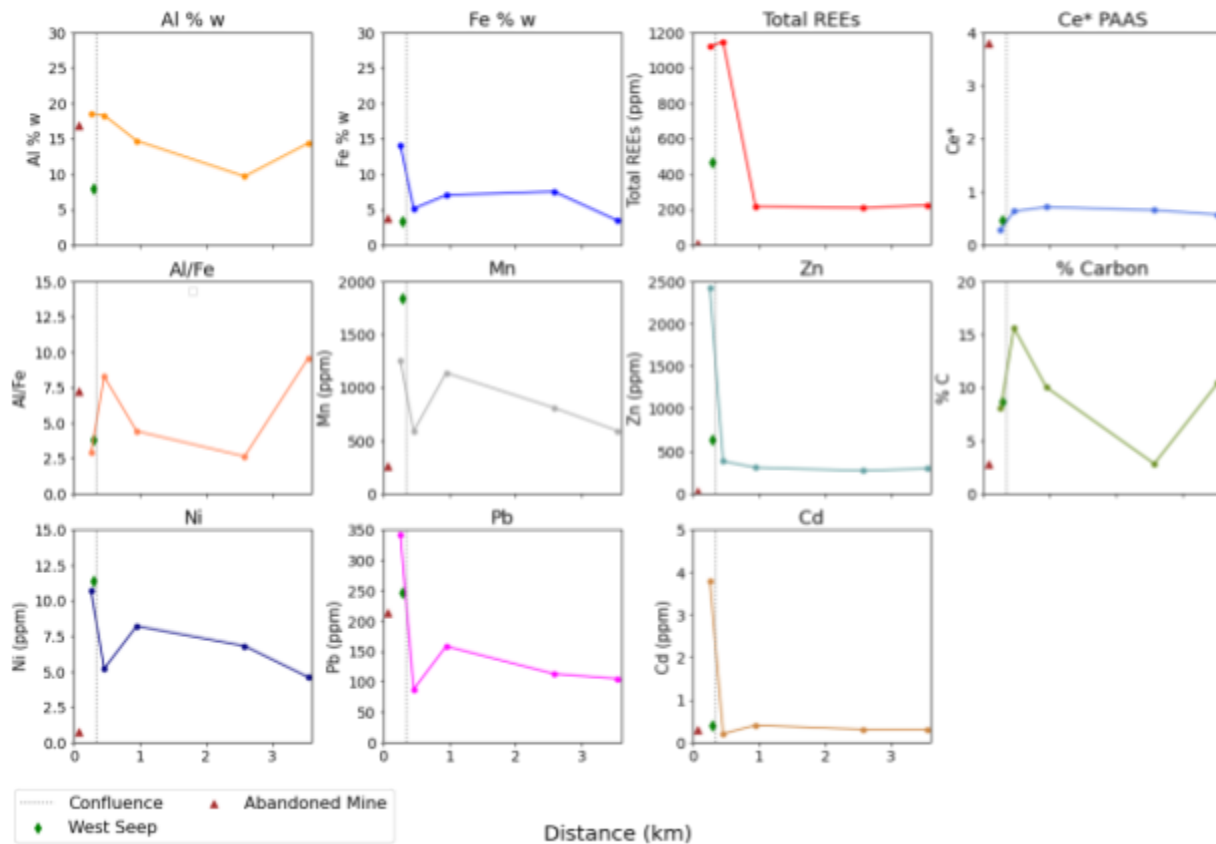


Figure 28. Flocculant chemistry of California Gulch. The gray dotted line represents the confluence of CG-Mine, CGS1, and CGS2 with the main stem of California Gulch.

Al and Fe had similar concentrations by weight (Figure 28). Most of the total REEs precipitated after their soluble input from CGS1. Low concentrations of total REEs in the precipitant from CGS2 indicate the source of total REEs in the flocculant downstream is from CGS1. All flocculant metals are higher and dropped after confluence. Flocculant concentrations for the mine were relatively low compared to other samples, except for Pb.

3.7 Flocculant Fe/Al and total REEs

Flocculant Al/Fe & Total REEs

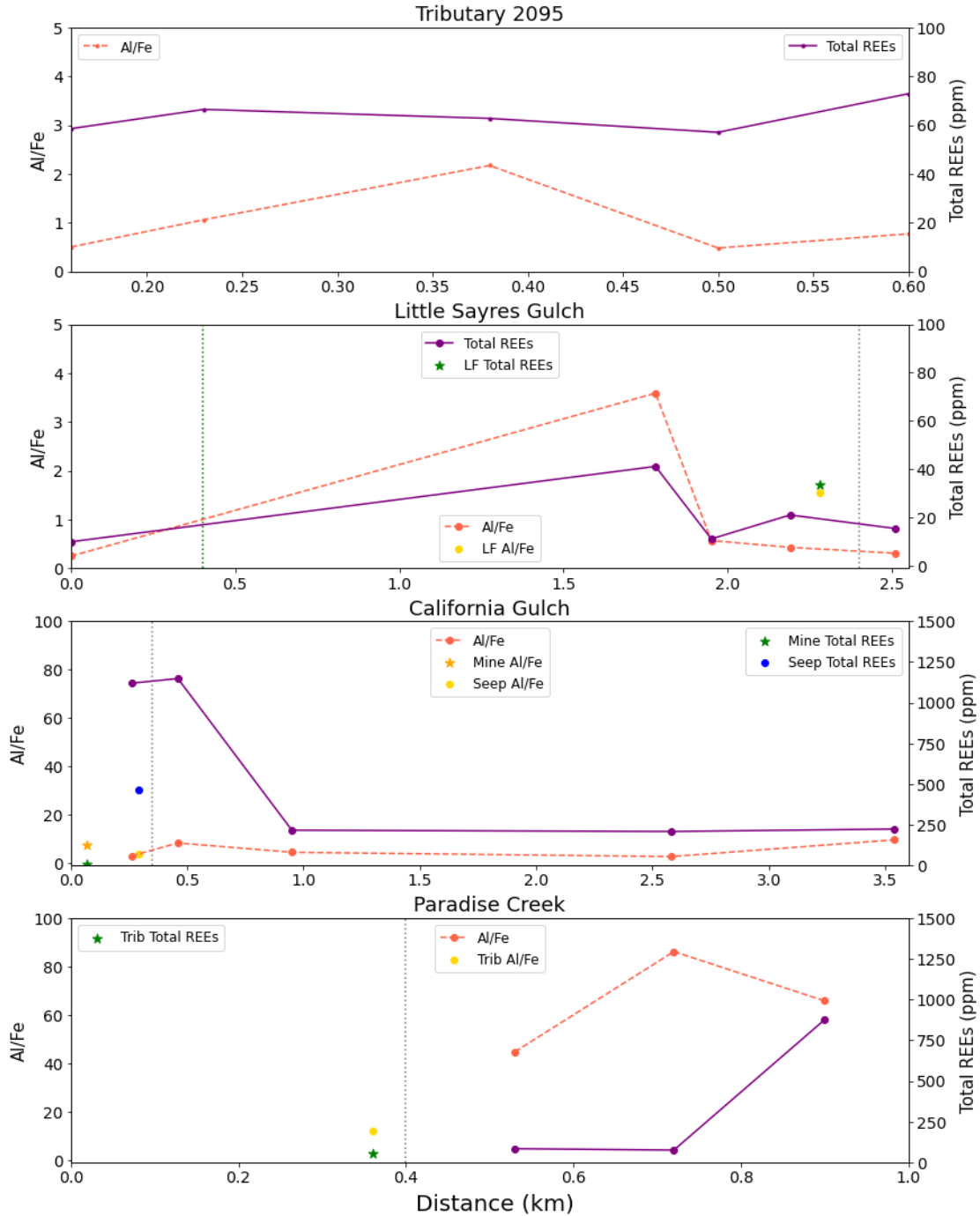


Figure 29. Relating Al/Fe to total REEs. Gray lines indicate confluences at the sample locations, and green lines indicate treeline.

The Al/Fe ratio vs. total REEs presents a coupled relationship in the synoptic study for all sites with available flocculant samples (Figure 29). California Gulch and Paradise Creek had higher Al/Fe values. These values indicated greater than a 1:1 ratio. These sites had high concentrations of total REEs ranging from 6.5-1150 ppm. Tributary 2095 and Little Sayres Gulch had low Al/Fe values of less than 5, indicating that they were higher in Fe than Al. These sites had relatively lower concentrations of total REEs less than 100 ppm.

3.8 Water Fluorescence Index and Flocculant Carbon/Nitrogen Ratio

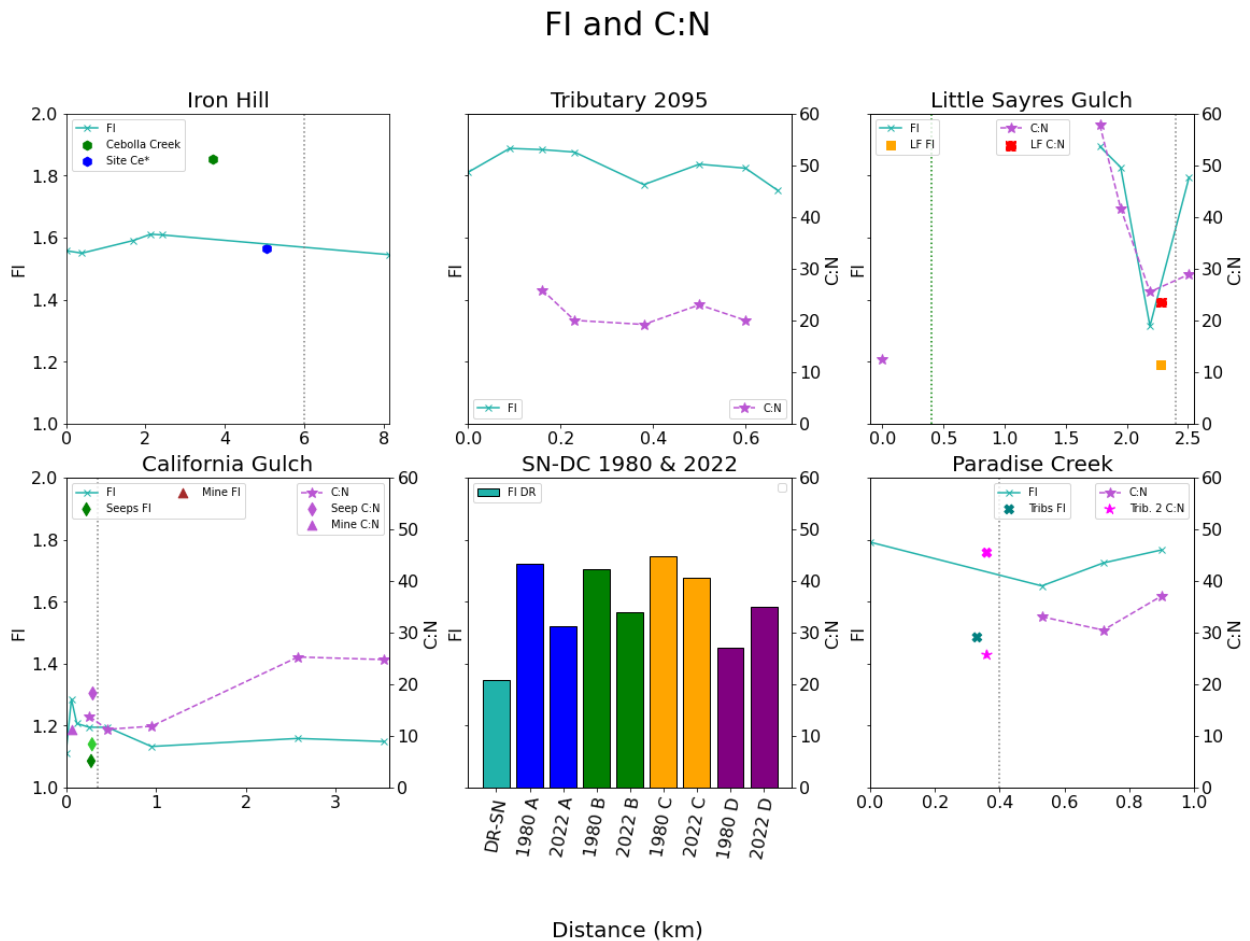


Figure 30. All sites comparing the water fluorescence index and flocculant carbon/nitrogen ratio.

Our control site Iron Hill did not have any precipitation and does not have C:N data (Figure 30). However, the FI values were generally within the range of 1.8 to 1.2 observed for DOM. Tributary 2095 had an FI close to 2 for the entire reach and a low C:N. Due to Fe fluorescence analysis interference, Little Sayres Gulch does not have FI data for the first three sites. Little Sayres Gulch FI and C:N collectively decreased prior to the confluence with LF. California Gulch has a low FI with increasing C:N. The FI for the SN-DC confluence is low. Comparing 1980 and 2022 C:N show a decrease for all flocculant sites but site D.

4.0 DISCUSSION

4.1 Water Chemistry

Iron Hill Water Chemistry

Known for its high REE concentrations in the carbonatite rock, Iron Hill's water chemistry had low concentrations of all metals, particularly Fe and Al. The chemical composition of carbonatite is >50% Calcite (CaCO_3) or dolomite ($\text{CaMg}(\text{CO}_3)_2$). The weathering of these minerals can buffer the adjacent surface water through dissolution and interaction with atmospheric CO_2 creating a basic pH and limiting the potential to leech and mobilize metals (Wen et al., 2022). This weathering also accounts for the increase of Ca as Beaver Creek flows north and begins to border Iron Hill and the decrease Ca after the confluence with Cebolla Creek where Ca concentrations were lower. Sulfate concentration increases post-confluence with Cebolla Creek and Deldorado Creek, likely from other sources upstream from the last sampling site. The spike in concentrations in BC3 and BC4 can be attributed to minimal slope and flow causing constituents to accumulate. There were no precipitates in this stream, so there is no flocculant data.

Tributary 2095 Water Chemistry

The consistent pH of ~3 in Tributary 2095 mobilized all metals at high concentrations. Sulfate acted conservatively, remaining around 2,400 mg/L while Fe decreased just below the treeline. The highest concentration of DOC occurred at the first sample site above the treeline indicating possible complexation and precipitation when progressing downstream. The pH is low and caused Al to remain in the solution. The most notable part of these data is the 3-fold increase of Fe, Al, Ni, Mn, Cd, Pb, Zn, and total REEs since the Rue 2012 data. This increase could be

attributed to a lower water table and changing climate conditions resulting in accelerated weathering as proposed by previous researchers (e.g. Crouch et al., 2013; Nordstrom, 2009; Todd et al., 2012; Zarroca et al., 2021). The 2022 sampling of Tributary 2095 was also done in the fall during low flow. It is possible that sample collection in either year could have occurred after a flushing event, which could elevate the concentrations. However, this increase is consistent with the continuing impacts of changing climate and hydrology.

Snake River-Deer Creek Confluence Water Chemistry

Comparing the recent available water chemistry of the Snake River-Deer Creek confluence showed changes over time at each component of the confluence. In the Snake River, there was a decrease in pH and increases of sulfate, Fe, Al, Zn, Cd, Mn, Pb, Ni, and a yearly increase of total REEs from 2021 to 2022. The lowered pH within the stream keeps Al in solution, and limits the sorption of trace metals. The confluence had these same trends between the data from Munk et. al., 2002, and our 2022 results of elevated concentrations compared to earlier data. Deer Creek had a decrease in DOC from 1990 to 2022. The shifts of increased metals could be attributed to lowered pH of the Snake River and the lower DOC of Deer Creek resulting in less Al oxide precipitation and therefore, increases in dissolved metals.

Little Sayres Gulch Water Chemistry

Little Sayres Gulch water chemistry is an ARD end member in this study. The very low pH indicates productive pyrite weathering. Indication of this weathering is the sulfate concentration exceeding 7000 mg/L, Fe above 1750 mg/L, and Al just below 1000 mg/L. Comparatively, the acceptable drinking water concentrations are 250 mg/L of Sulfate, 0.5-1 mg/L of Fe, and 0.05-2 mg/L of Al (CDC, 2021). Ni, Pb, and Cd exceed standards as well. The

high amount of precipitation of oxides within the stream can be related to the high concentrations and saturated conditions. Most all metals decrease drastically below treeline when DOC concentrations increase and completely leave the solution phase of the system after the confluence with Left Fork Lake Creek. Uniquely, REEs remain around 1000 ppb until after the confluence. This indicates that within this stream the total REEs act conservatively regardless of increased DOC concentrations which seem to have affected other dissolved metals. This observation agrees with Verplanck et al (2004) who found using REEs as a conservative tracer is only reliable with a pH lower than 5.1.

Paradise Creek Water Chemistry

The Verplanck et al (2004) finding is also consistent with Paradise Creek results where REE concentration begins to decrease once pH reaches just above 5. This is the only location with an increase in pH. This increase occurred after the confluence of PCT1 and PCT2 to the main stem of Paradise Creek. The initially higher pH of these tributaries are the cause of the increase of pH in the main stem. The Fe content was below detection, which is explained by the higher pH of 4.5 - Fe is only soluble under 4 pH. The pH is not low enough to mobilize the Fe. There is an inverse relationship between pH and most all the other metals showing the control pH has within the system on solubility and precipitation. When comparing downstream sites (PC2, PC3, PC4) within the marshy reach the DOC content also decreases. This pattern is likely due to precipitation of oxides on the stream bed and complexation with metals as the pH increases.

California Gulch Water Chemistry

California Gulch has complex hydrology within its reaches. During sampling two seeps and the abandoned mine/adit (CG-Mine) were sampled in addition to the main stem. However, at least 5-6 more seeps were observed with very low flow. These distributed inputs can create dynamic changes in chemistry downstream. California Gulch pH lowered below its confluence with the seeps and CG-Mine. These inputs greatly affect the chemistry of the stream. The low pH and Fe input from CG-Mine and high total REEs (1398 ppb) from the eastern seep are examples of the influence of these inputs as the main stem enters the marsh environment, DOC increased and all metals, except Fe decreased. The Fe concentrations were less than 0.2 mg/L in the main stem and California Gulch is Al dominant.

Water: Cerium Anomaly

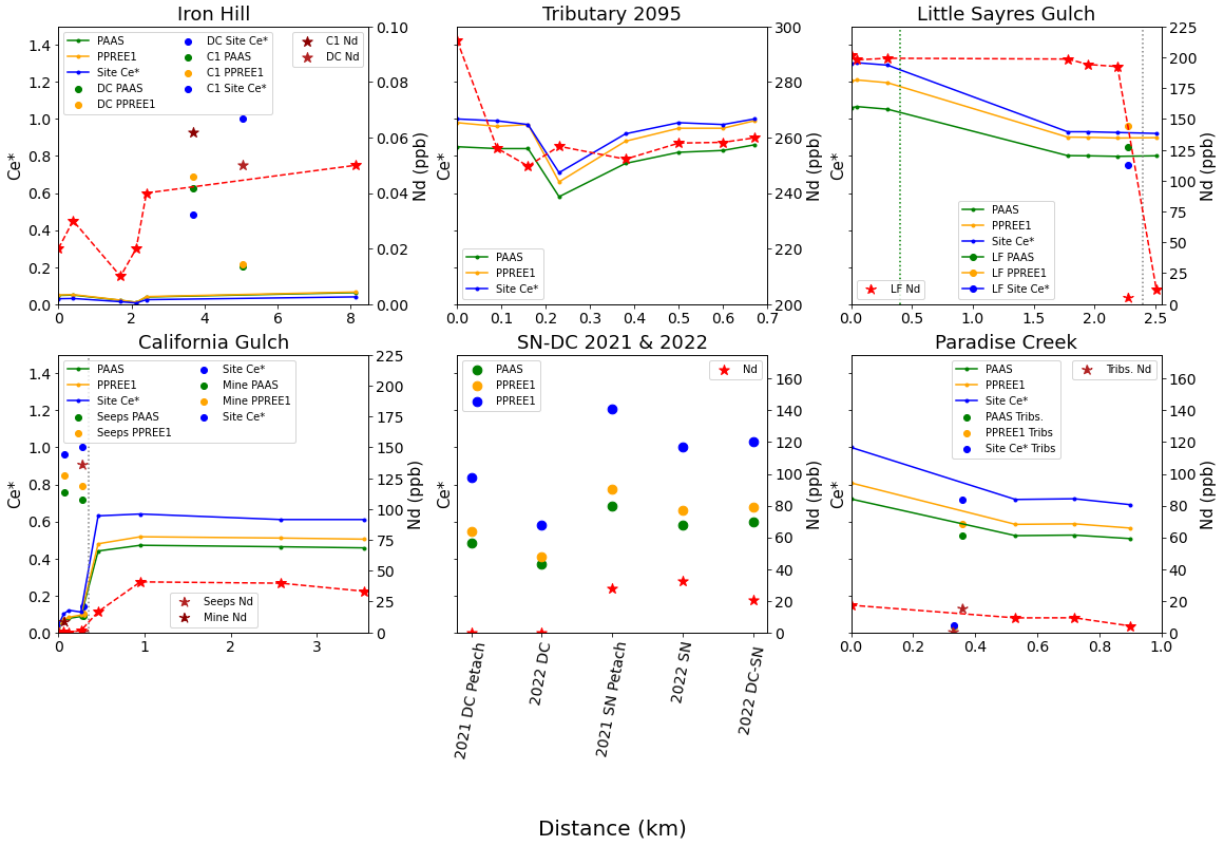


Figure 31. All locations calculations of the cerium anomaly (Ce*) with three different standardizations compared to the Nd concentrations.

Using multiple standardizations to calculate the Ce anomaly (Ce*) illustrates the influence each approach has on representing the relative abundance of Ce to its neighboring elements (Figure 31). Standardizing water samples to the PAAS, a rock standard, seems to be less representative of the water itself and consistently gives lower values. Whereas standardizing water samples to the site PPREE1 (Figure 31 (yellow)) a high-altitude stream portal is well within the realm of this study. Standardizing to the site with the highest REEs within the specific location

emphasizes the relationship within the site itself rather than a less comparable standard. In all cases, they follow the same trend per location.

All Ce* indicate more positive values and reducing conditions in the initial reaches, except for Iron Hill and California Gulch. These are as expected. Iron Hill has a high pH and low metal concentrations. California Gulch received most of its REE concentration from seep 1 which is why the Ce* increases after the confluence based on relative abundance. The decreases in Ce* indicate the conditions become more oxidizing as the stream continues downstream, thus making Ce insoluble.

Most sites show a similar trend of Ce* and Nd when going downstream. However, high Fe sites, e.g. Tributary 2095, and Little Sayres Gulch, have differing downstream trends with Nd compared to all other sites. This could be explained by the “oxidation scavenging” of Ce by Fe oxides (Liu et al., 2017; Pourret & Davranche, 2013; Ratié et al., 2020). This scavenging process by Fe oxide takes Ce out of solution by oxidizing it from Ce (III) to insoluble Ce (IV). This process would explain the lack of similarity.

4.2 Flocculant Chemistry

Tributary 2095 Flocculant

The flocculant within Tributary 2095 had consistent REEs that slightly increased at the end of the reach. The water pH slightly increased at this stage as well which could be attributed to the increase in REE concentration within the flocculant. This also occurred for other metals, Pb, Cd, Mn, Ni, supporting increased precipitation with increased pH. The flocculant within Tributary 2095 was more brittle and dense as a result of the low pH and high Fe concentrations.

Speciation of Fe is assumed to be an amorphous Fe mineral (e.g. FeO(OH)) rather than hydrous iron oxide in nature.

Snake River-Deer Creek Confluence Flocculant Comparison

Comparison of sites A-D in the Snake River and Deer Creek confluence between flocculant collected in 1980 and 2022 indicated a decrease in all trace metals associated with the flocculant hydrous metal oxides. This trend includes a decrease in total REEs from a maximum of 425 ppm to 101 ppm in 42 years. The exception to this is Al and Fe. In 1980, the flocculant at SN-DC was dominated by Al, however, the flocculant was dominated by Fe in 2022. This shift may be attributed to the lowering pH in the Snake River, causing more Fe to mobilize and leave more Al in solution at the confluence.

The decrease of other trace metals can then be attributed to the photoreduction of Fe in the confluence. As seen in (Figure 9), the confluence is not shaded and open to UV radiation. This solar radiation can cause the photoreductive dissolution of iron oxides, releasing not only the ferrous iron but also any other sorbed species. The nature of the flocculant is a light, velutinous consistency when compared to the more upstream flocculant of Tributary 2095. This is likely stems from the higher pH creating more favorable conditions for hydrous metal oxide speciation over densely amorphous speciations.

Little Sayres Gulch Flocculant

Flocculant concentrations in Little Sayres Gulch differed between the first portal site above the treeline and the next sites all below the treeline. Al content remains relatively low. Variations of all constituents could be attributed to the photoreduction of iron (McKnight & Bencala, 1988). The site with the highest concentration of metals (LS4) was adjacent to deep

shaded forest. By comparison to other sites, this site could have less UV-radiation, exposure leading to greater stability, and accumulation in the hydrous iron oxides. Comparing these concentrations to the more open downstream sites, there is a drop in concentrations. Post-confluence with Left Fork Lake Creek represents how the quick increase in pH increases the metal concentrations in the flocculant. This pH increase also changed the nature of the flocculant, resulting in flocculant with a gossamer texture. Where as the upper reaches of Little Sayres Gulch had very dense and more friable flocculant, so much so, that cobbles were difficult to remove from the stream bed due to the dense precipitation.

Paradise Creek Flocculant

Paradise Creek is dominated by Al oxide precipitation. This dominance by Al is apparent by its white stream bed. The flocculant chemistry supports the water chemistry concentration decreases which can be attributed to the precipitation of the oxides. Most all trace metals continue to increase in the marshy reaches. Paradise Creek's last sample site (PC4) had the highest concentration of total REEs in this study at 876 ppm. The high aluminum and carbon concentration could have been attributed to the preferential sorption of REEs onto Al oxides and the complexation and sorption of Al oxides with DOC. The low concentration of Fe in the flocculant indicates a lack of Fe photoreductivity resulting in a greater residence time for trace metals within the flocculant is longer and has the potential for concentration to accumulate progressing downstream. The high concentration of REEs in the most downstream sample site is likely to cause the decrease in Ce* because Ce* is relative to atomically adjacent REEs, La, and Pr. A shift in La and Pr concentrations can cause a decrease in Ce*.

California Gulch Flocculant

The flocculant in California Gulch is relatively enriched in Al but to a lesser extent than in Paradise Creek. Total REEs in the flocculant are stable after the pH of the main stem decreases to under 5.0. This is also the case for Zn and Cd. The mobilization of these metals seemed to precipitate after the confluence and then became more evenly distributed. The consistent increase of DOC and leveling of pH would explain this pattern. The spike in Mn, Pb, and Ni around 1 km can be described by the complexation of high metal inputs from CGS1 downstream.

4.3 Aluminum, Iron, and Total REE Relationships

When comparing the flocculant results for all sites (except Iron Hill) there is an observable relationship between the concentration of REEs in Al-rich flocculant vs. Fe-rich flocculant (Figure 29). The number of samples with a low total REE concentration is higher than those with high REE concentrations (Figure 32). However, the number of samples with low Al is less (Figure 33). An Al/Fe ratio was calculated for each site to determine the extent of this relationship. Putting this in $\log(\text{Al/Fe})$ form it is easier to observe the number of sites dominant in Al vs. Fe (Figure 34). To assess whether there is a statistically significant difference between the amount of REEs in Al dominant vs. Fe dominant sites I ran a two-sample t-test using R-Studio statistical software. This produced a p-value of $7.39e^{-3}$ with a 95% confidence. The significance of the analysis indicates the greater control of the sorption of REEs is due to Al concentrations in the flocculant rather than Fe concentrations.

Total REEs Flocculant Concentration Sample Distribution

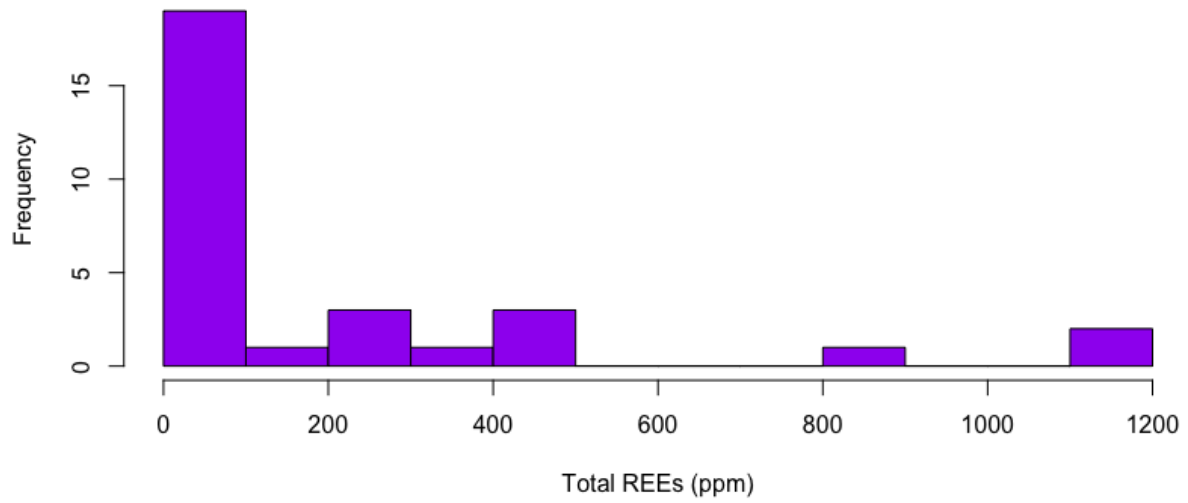


Figure 32. Distribution of total REE concentrations in each sample.

Flocculant Sample Al Percent

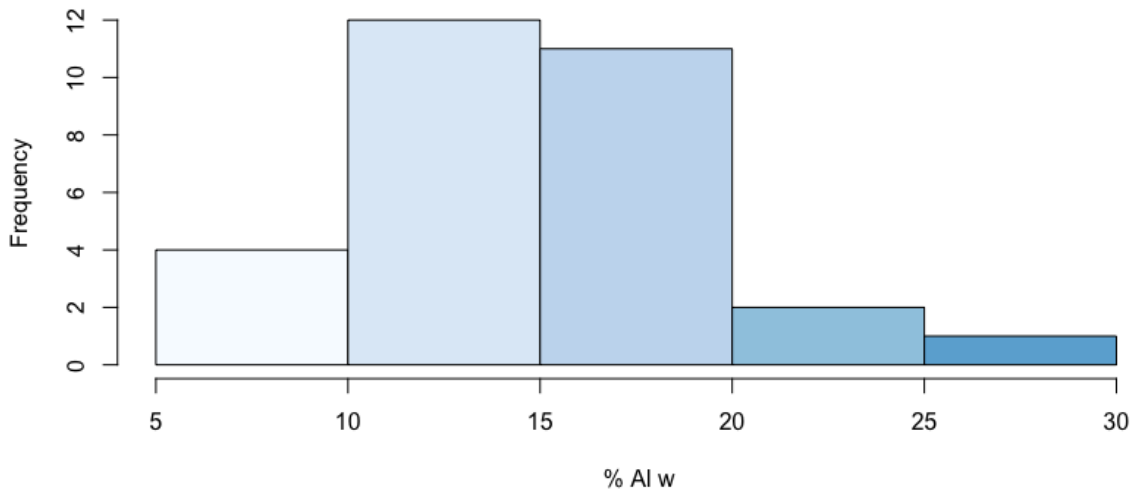


Figure 33. Sample distribution of percent Al concentrations.

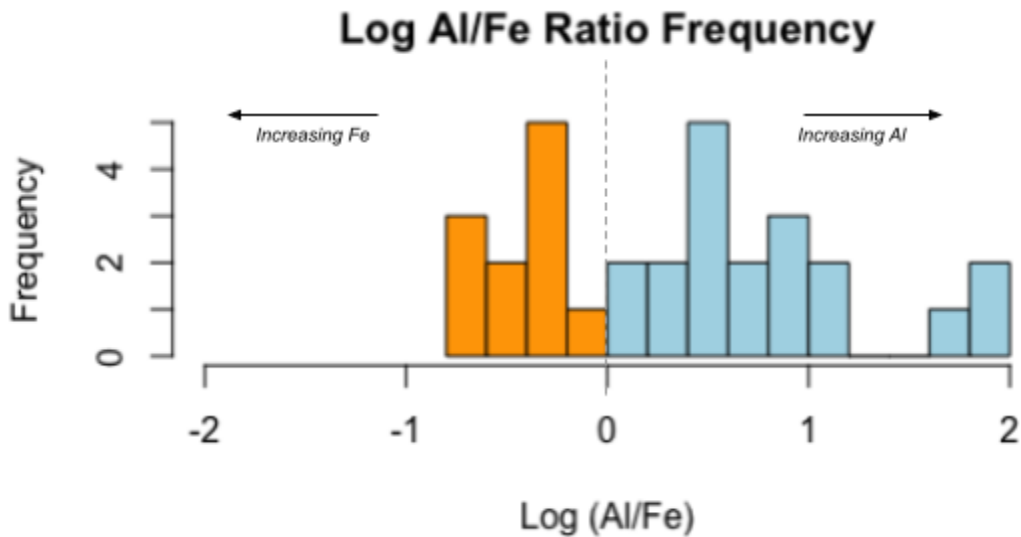


Figure 34. Sample frequency of log ratio of Al/Fe.

4.4 Fluorescence Index and Carbon/Nitrogen Ratio

An FI between ~ 1.8 indicates microbially derived DOM and ~ 1.2 is soil/plant litter driven (Gabor et al., 2014; McKnight et al., 2001). Comparably a C:N of 8 indicated microbially driven, 11 is humus, and 14.8 is terrestrial riverine input (Prahl et al., 1994; Schwyter & Vaughan, 2021). It is no surprise that FI and C:N follow the same trends as they are both representative of organic matter characteristics. The higher C:N for Little Sayres is below the treeline, whereas the first site is very low indicating microbial influence. California Gulch has low FI and C:N which is a different relationship. The C:N indicates a microbial input in the upper reaches, whereas the FI indicates terrestrial input. Comparison data for the SN-DC indicate the ratio of C:N is decreasing, however, these are still indicative of terrestrial input. The FI for this site supports this interpretation. Paradise Creek indicates a terrestrial input increase in C:N in the lower reaches and more microbial input from the FI.

One important distinction when comparing the FI and C:N is the FI represents water composition and the C:N represents the flocculant composition. Contradictions of source could

be attributed to the DOC sources preferentially staying in the water or sorbing. Fulvic acid that is more “sorbable” is generally richer in N (McKnight et al., 2002). This relationship could skew the classification for C:N in the flocculant. Further examination is required to determine the extent of these relationships.

Location	Site	pH	Summer 2022			Flocculant Percent by Weight				Molar Ratio Al/Fe
			Dissolved Fe in Water (mg/L)	% Fe w/w	% Al w/w	% Fe as Fe(OH) ₃ or *FeO(OH)	% Al as Al(OH) ₃	Total Carbon %	Total	
CA Gulch	CG-MINE	3.35	9.1	2.4	5.8	3.8	16.9	2.8	23.5	7.2
	CGS2-Mid	5.92	0	1.7	6.4	3.3	7.9	8.6	19.8	3.82
	CG-4	6.21	0	7.4	6.3	14.1	18.5	17.8	50.4	2.88
	GC-5	5.53	0	2.7	5.1	5.1	18.3	1.8	25.2	8.24
	CG-6	4.67	0	3.7	3.3	7	14.7	7.6	29.3	4.4
	CG-7	5.11	0.1	4.0	5.0	7.5	9.7	9.6	26.8	2.62
	CG-8	5.08	0.2	1.8	4.8	3.4	14.3	7.2	24.9	9.54
2095	2095-3	2.99	162.8	25.9	5.3	41.4*	13.8	15	70.2	0.5
	2095-4	3	203.6	13.3	2.3	21.3*	15.4	3.6	40.3	1.06
	2095-5	2.98	158.2	5.7	6.7	9.1*	6.8	5	20.9	2.17
	2095-6	2.94	187.7	36.6	4.8	58.6*	19.4	6.2	84.2	0.48
	2095-7	2.91	112.8	12.6	6.4	20.2*	14.0	4.8	39.0	0.77
Little Sayres	LS1	2.68	1718	72.2	4.8	115.4*	18.4	8	141.8	0.25
	LS4	2.95	301	5.6	2.6	8.9*	13.9	15.6	38.4	3.59
	LS5	2.97	280	13.6	6.7	21.7*	7.5	10	39.2	0.57
	LS6	2.93	270.7	40.8	4.6	65.2*	19.4	2.8	87.4	0.43
	LS7	3.7	3.8	71.1	5.1	134.4	13.3	10.4	158.1	0.31
	LF	4.59	10.9	8.9	7.6	16.9	18.8	14.8	50.5	1.56
Paradise Creek	PCT2	4.98	0	2.2	6.3	4.2	21.8	3.6	29.6	11.73
	PC2	5.13	0	0.5	2.7	1	14.9	8.6	24.5	44.71
	PC3	5.15	0	0.4	4.5	0.7	18.2	6.4	25.3	86.2

	PC4	5.76	0	0.4	4.7	0.8	16.9	17.8	35.5	65.8
Confluence 1980	SN-A	4.5-6 McKnight et al., 1992	--	4.5	4.3	8.5	12.9	33	54.4	3.59
	SN-B		--	4.1	6.0	7.7	13.6	35.2	56.5	2.21
	SN-C		--	1.4	4.4	3.3	12.5	33.2	49.0	5.19
	SN-D		--	3.2	7.4	6.1	12.7	10	28.8	10.24
Confluence 2022	SN-DC A	3.71	0.4	74.7	10.4	119.5	21.5	20	161.0	0.33
	SN-DC B			107.5	5.5	172	30.0	24.8	226.8	0.25
	SN-DC C			35.8	3.9	57.2	15.8	24.8	97.8	0.48
	SN-DC D			48.7	5.8	77.9	11.2	14	103.1	0.2

Table 2. Flocculant data compared to water pH and dissolved Fe content. An asterisk indicates when FeO(OH) was assumed as the speciation of Fe associated with low (<3.5) pH. Orange highlights indicate overly high percent iron concentrations.

4.5 Variable Weight Percentages of Flocculant

It is recognized that the major constituents of the flocculant at many of the sites do not sum to substantial (e.g. >50%) weight percentages even when the Fe and Al values are used to calculate the percentage by weight of the hydrous metal oxide as was expected. This analytical result could be attributed to the digestive method which did not use hydrofluoric acid, such that undigested grains were observed for all samples. These grains were qualitatively evaluated and consisted of a range of mineral materials (e.g. silicas, feldspars, pyroxenes). These mineral grains have a density ranging from 2.62-3.9 g/cm³ which could account for greater portion of the weight than less dense hydrous metal oxides (e.g. 2.42-3.4 g/cm³).

A distinction of the assumed flocculant Fe speciation was based on water pH. For flocculant samples originating from stream water with a pH > 3.5 it is assumed the majority of Fe speciated as hydrous iron oxide (Fe(OH)₃). For flocculant samples from an environment with a pH of <3.5 it is assumed iron precipitated as lepidocrocite, goethite, or other densely crystalline amorphous species (FeO(OH)). In addition to pH, the textural nature of these samples led to using FeO(OH) as the speciation (Table 2. Indicated by asterisks). This flocculant was denser and more friable, where as, samples dominated by hydrous metal oxides in an environment with a pH >3.5 the flocculant was lighter and more velutinous.

There are four samples with overly high hydrous iron oxide content: LS1, LS7, 2022 SN-DC A and B (Table 2. highlighted in orange). The overly high oxide content could reflect: (1) A denser iron speciation for lower pH samples would have a higher Fe content with a lower hydroxyl content. (2) Fe³⁺ or Fe²⁺ ions sorbing onto Al hydrous oxide while interacting possibly by strong complexation reactions with fulvic acid ligands. The reaction of Fe hydrous oxides

with certain types of fulvic acid can reduce the kinetic reaction of the photodegradation causing the iron oxides to age and become denser and more crystalline (Hncir and McKnight, 1998).

5.0 CONCLUSIONS

Decadal comparisons in the Snake River watershed indicate that there are temporal changes happening within this watershed. Within a decade, Tributary 2095 had a 3-fold increase in metal concentrations from 2009 to 2022. Given there is no direct anthropogenic influence on this stream, the increase can be attributed to a warming climate and lowered water table giving way to accelerate the ARD process. Furthering the trend of temporal comparison is the shifts in water chemistry in the SN-DC confluence where there were decreases in pH and increases in metal concentrations.

Perhaps the most revealing result from this study is the decrease in metal concentrations in the SN-DC flocculant, particularly, total REEs. This indicates higher concentrations of REEs in flocculant were typical, but the processes controlling their sorption have shifted. Decreases in pH and increases in Fe concentrations allow total REEs to mobilize further downstream rather than sorb onto the stream bed. Further investigation and comparison of the sites indicate the controlling factor of REE sorption is not DOC. While DOC makes contributions to the sorption of trace metals and REEs, it seems the main controlling factor is the abundance of Al oxides over Fe oxides. Statistical analysis with the data from all flocculant sites supports this observation.

The shift from Al-dominant flocculant to Fe-dominant from 1980 to 2022 sets the stage for possible shifts in other Al-dominant streams in the future. This study supports Al dominant streams as a better sink for metal precipitation. Conditions supporting otherwise, like Fe dominant systems, can cause trace metals to mobilize further downstream possibly increasing environmental and water quality issues.

6.0 REFERENCES

- Bierens de Haan, S. (1991). A review of the rate of pyrite oxidation in aqueous systems at low temperatures. *Earth-Science Reviews*, 31(1), 1–10.
[https://doi.org/10.1016/0012-8252\(91\)90039-I](https://doi.org/10.1016/0012-8252(91)90039-I)
- Bird, D., Sares, M., Peters, D., Hauff, P., Coulter, D., & Iii, F. (2005). *NATURALLY OCCURRING ACID ROCK DRAINAGE IN COLORADO'S LAKE CREEK WATERSHED* (Vol. 2005). <https://doi.org/10.21000/JASMR05010071>
- Brooks, P. D., McKnight, D. M., & Bencala, K. E. (1999). The relationship between soil heterotrophic activity, soil dissolved organic carbon (DOC) leachate, and catchment-scale DOC export in headwater catchments. *Water Resources Research*, 35(6), 1895–1902.
<https://doi.org/10.1029/1998WR900125>
- CDC. (2021). *Toxic Substances*. Toxic Substances. <https://wwwn.cdc.gov/TSP/index.aspx>
- Crouch, C. M., McKnight, D. M., & Todd, A. S. (2013). Quantifying sources of increasing zinc from acid rock drainage in an alpine catchment under a changing hydrologic regime. *Hydrological Processes*, 27(5), 721–733. <https://doi.org/10.1002/hyp.9650>
- Dudley, J. L., Arthurs, W., & Hall, T. J. (2001). A Comparison of Methods Used to Estimate River Rock Surface Areas. *Journal of Freshwater Ecology*, 16(2), 6.
- Fridrich, C. J., Smith, R. P., Dewitt, E., & Mckee, E. H. (1991). Structural, eruptive, and intrusive evolution of the Grizzly Peak caldera, Sawatch Range, Colorado. *Geological Society of America Bulletin*, 103(9), 1160–1177.
[https://doi.org/10.1130/0016-7606\(1991\)103<1160:SEAIEO>2.3.CO;2](https://doi.org/10.1130/0016-7606(1991)103<1160:SEAIEO>2.3.CO;2)
- Gabor, R., Baker, A., McKnight, D. M., & Miller, M. (2014). *Fluorescence Indices and Their*

Interpretation. Aquatic Organic Matter Fluorescence.

- Harahuc, L., Lizama, H. M., & Suzuki, I. (2000). Selective Inhibition of the Oxidation of Ferrous Iron or Sulfur in *Thiobacillus ferrooxidans*. *Applied and Environmental Microbiology*, *66*(3), 1031–1037.
- Hrcncir, D. C., & McKnight, D. (1998). Variation in photoreactivity of iron hydroxides taken from an acidic mountain stream. *Environmental Science & Technology*, *32*(14), 2137–2141.
<https://doi.org/10.1021/es970986l>
- Lawaetz, A., & Stedmon, C. (2009). Fluorescence Intensity Calibration Using the Raman Scatter Peak of Water. *Applied Spectroscopy*, *63*, 936–940.
<https://doi.org/10.1366/000370209788964548>
- Liu, H., Pourret, O., Guo, H., & Bonhoure, J. (2017). Rare earth elements sorption to iron oxyhydroxide: Model development and application to groundwater. *Applied Geochemistry*, *87*, 158–166. <https://doi.org/10.1016/j.apgeochem.2017.10.020>
- Malhotra, N., Hsu, H.-S., Liang, S.-T., Roldan, M. J. M., Lee, J.-S., Ger, T.-R., & Hsiao, C.-D. (2020). An Updated Review of Toxicity Effect of the Rare Earth Elements (REEs) on Aquatic Organisms. *Animals*, *10*(9), Article 9. <https://doi.org/10.3390/ani10091663>
- Manning, A. H., Verplanck, P. L., Caine, J. S., & Todd, A. S. (2013). Links between climate change, water-table depth, and water chemistry in a mineralized mountain watershed. *Applied Geochemistry*, *37*, 64–78. <https://doi.org/10.1016/j.apgeochem.2013.07.002>
- McKnight, D. M., & Bencala, K. E. (1988). Reactive iron transport in an acidic mountain stream in Summit County, Colorado: A hydrologic perspective. *Geochimica et Cosmochimica Acta*, *53*(9), 2225–2234. [https://doi.org/10.1016/0016-7037\(89\)90346-3](https://doi.org/10.1016/0016-7037(89)90346-3)
- McKnight, D. M., & Bencala, K. E. (1990). The Chemistry of Iron, Aluminum, and Dissolved

- Organic Material in Three Acidic, Metal-Enriched, Mountain Streams, as Controlled by Watershed and in-Stream Processes. *Water Resources Research*, 26(12), 3087–3100.
<https://doi.org/10.1029/WR026i012p03087>
- McKnight, D. M., Bencala, K. E., Zellweger, G. W., Aiken, G. R., Feder, G. L., & Thorn, K. A. (1992). Sorption of dissolved organic carbon by hydrous aluminum and iron oxides occurring at the confluence of Deer Creek with the Snake River, Summit County, Colorado. *Environmental Science & Technology*, 26(7), 1388–1396.
<https://doi.org/10.1021/es00031a017>
- McKnight, D. M., Boyer, E. W., Westerhoff, P. K., Doran, P. T., Kulbe, T., & Andersen, D. T. (2001). Spectrofluorometric characterization of dissolved organic matter for indication of precursor organic material and aromaticity. *Limnology and Oceanography*, 46(1), 38–48.
<https://doi.org/10.4319/lo.2001.46.1.0038>
- McKnight, D. M., Hornberger, G. M., Bencala, K. E., & Boyer, E. W. (2002). In-stream sorption of fulvic acid in an acidic stream: A stream-scale transport experiment. *Water Resources Research*, 38(1), 6-1-6–12. <https://doi.org/10.1029/2001WR000269>
- METHOD 7000B FLAME ATOMIC ABSORPTION SPECTROPHOTOMETRY*. (2007).
Environmental Protection Agency.
<https://www.epa.gov/sites/default/files/2015-12/documents/7000b.pdf>
- Mining and Water Quality*. (n.d.). USGS. Retrieved December 2, 2022, from
<https://www.usgs.gov/faqs/how-does-mine-drainage-occur>
- Munk, L., Faure, G., Pride, D. E., & Bigham, J. M. (2002). Sorption of trace metals to an aluminum precipitate in a stream receiving acid rock-drainage; Snake River, Summit County, Colorado. *Applied Geochemistry*, 17(4), 421–430.

[https://doi.org/10.1016/S0883-2927\(01\)00098-1](https://doi.org/10.1016/S0883-2927(01)00098-1)

- Nordstrom, D. K. (2009). Acid rock drainage and climate change. *Journal of Geochemical Exploration*, 100(2–3), 97–104. <https://doi.org/10.1016/j.gexplo.2008.08.002>
- Oliás, M., Cánovas, C. R., Basallote, M. D., & Lozano, A. (2018). Geochemical behaviour of rare earth elements (REE) along a river reach receiving inputs of acid mine drainage. *Chemical Geology*, 493, 468–477. <https://doi.org/10.1016/j.chemgeo.2018.06.029>
- Pagano, G. (2017). *Rare earth elements in human and environmental health: At a crossroads between toxicity and safety*. Pan Stanford Publishing.
- Pagano, G., Guida, M., Tommasi, F., & Oral, R. (2015). Health effects and toxicity mechanisms of rare earth elements—Knowledge gaps and research prospects. *Ecotoxicology and Environmental Safety*, 115, 40–48. <https://doi.org/10.1016/j.ecoenv.2015.01.030>
- Payne, M. (n.d.). *100summits—Elk Mountains*. Retrieved November 30, 2022, from <http://www.100summits.com/articles/ranges/item/128-elk-mountains>
- Petach, T. (2022). *Remediation of acid rock drainage in a changing climate: Assessment of bulkhead closures and long-term water quality trends in the Colorado Mineral Belt* [Ph.D.]. University of Colorado Boulder.
- Pourret, O., & Davranche, M. (2013). Rare earth element sorption onto hydrous manganese oxide: A modeling study. *Journal of Colloid and Interface Science*, 18–23. <https://doi.org/10.1016/j.jcis.2012.11.054>
- Prahl, F. G., Ertel, J. R., & Goni, M. A. (1994). Terrestrial organic carbon contributions to sediments on the Washington margin. *Geochemica et Cosmochimica Acta*, 58(14), 3035–3048. [https://doi.org/10.1016/0016-7037\(94\)90177-5](https://doi.org/10.1016/0016-7037(94)90177-5)
- Ratié, G., Vantelon, D., Pédrotb, M., Beauvois, A., Chaouchi, K., Fosséc, C., & Davranche, M.

- (2020). Cerium anomalies in riverbanks: Highlight into the role of ferric deposits. *Science of The Total Environment*, 713. <https://doi.org/10.1016/j.scitotenv.2020.136544>
- Redfield, A. C. (1958). The Biological Control of Chemical Factors in the Environment. *American Scientist*, 46(3), 230A – 221.
- Rue, G. P., & McKnight, D. M. (2021). Enhanced Rare Earth Element Mobilization in a Mountain Watershed of the Colorado Mineral Belt with Concomitant Detection in Aquatic Biota: Increasing Climate Change-Driven Degradation to Water Quality. *Environmental Science & Technology*, 55(21), 14378–14388. <https://doi.org/10.1021/acs.est.1c02958>
- Schwytter, A., & Vaughan, K. (2021). *Carbon/Nitrogen Ratio*. Geosciences LibreTexts. [https://geo.libretexts.org/Bookshelves/Soil_Science/Introduction_to_Soil_Science_Laboratory_Manual_\(Schwyter_and_Vaughan\)/10%3A_Soil_Ecology/10.05%3A_Carbon_Nitrogen_Ratio](https://geo.libretexts.org/Bookshelves/Soil_Science/Introduction_to_Soil_Science_Laboratory_Manual_(Schwyter_and_Vaughan)/10%3A_Soil_Ecology/10.05%3A_Carbon_Nitrogen_Ratio)
- Singer, P. C., & Stumm, W. (1970). Acidic Mine Drainage: The Rate-Determining Step. *Science*, 167(3921), 1121–1123.
- Skidmore, J. F. (1964). Toxicity of Zinc Compounds to Aquatic Animals, with Special Reference to Fish. *The Quarterly Review of Biology*, 39(3), 227–248. <https://doi.org/10.1086/404229>
- Theobald, P. K., Lakin, H. W., & Hawkins, D. B. (1963). The precipitation of aluminum, iron and manganese at the junction of Deer Creek with the Snake River in Summit County, Colorado. *Geochimica et Cosmochimica Acta*, 27(2), 121–132. [https://doi.org/10.1016/0016-7037\(63\)90053-X](https://doi.org/10.1016/0016-7037(63)90053-X)
- Todd, A., Manning, A., Verplanck, P., Crouch, C., Mcknight, D., & Dunham, R. (2012).

- Climate-Change-Driven Deterioration of Water Quality in a Mineralized Watershed.
Environmental Science & Technology, 46, 9324–9332. <https://doi.org/10.1021/es3020056>
- US EPA, O. (2015, November 30). *National Primary Drinking Water Regulations* [Overviews and Factsheets].
<https://www.epa.gov/ground-water-and-drinking-water/national-primary-drinking-water-regulations>
- USGS Mineral Resources Program. (2014). *The Rare-Earth Elements—Vital to Modern Technologies and Lifestyles* (Fact Sheet) [Fact Sheet]. USGS.
- Van Gosen, B. (2009). *The Iron Hill (Powderhorn) Carbonatite Complex, Gunnison County, Colorado—A Potential Source of Several Uncommon Mineral Resources* (Open-File Report No. 1005; Open-File Report). U.S. Geological Survey, U.S. Department of the Interior.
- Verplanck, P. L., Nordstrom, D. K., & Taylor, H. E. (1999). *Overview of Rare Earth Element Investigations in Acid Waters of U. S. Geological Survey Abandoned Mine Lands Watersheds* (US Geological Survey Water Resource Investigations No. 4018A; p. 10). USGS.
- Verplanck, P. L., Nordstrom, D. K., Taylor, H. E., & Kimball, B. A. (2004). Rare earth element partitioning between hydrous ferric oxides and acid mine water during iron oxidation. *Applied Geochemistry*, 19(8), 1339–1354.
<https://doi.org/10.1016/j.apgeochem.2004.01.016>
- Washington, J. (2016). *Geochemical Considerations Regarding the Gold King Mine Release*.
- Wen, H., Sullivan, P. L., Billings, S. A., Ajami, H., Cueva, A., Flores, A., Hirmas, D. R., Koop, A. N., Murenbeeld, K., Zhang, X., & Li, L. (2022). From Soils to Streams: Connecting

Terrestrial Carbon Transformation, Chemical Weathering, and Solute Export Across Hydrological Regimes. *Water Resources Research*, 58(7), e2022WR032314.

<https://doi.org/10.1029/2022WR032314>

Williams, F., & Chronic, H. (2014). *Roadside geology of Colorado* (Third edition). Mountain Press Publishing Company.

Zarroca, M., Roqué, C., Linares, R., Salminci, J. G., & Gutiérrez, F. (2021). Natural acid rock drainage in alpine catchments: A side effect of climate warming. *Science of The Total Environment*, 778, 146070. <https://doi.org/10.1016/j.scitotenv.2021.146070>

7.0 APPENDIX AND SUPPLEMENTARY MATERIAL

Sulfate Relationships

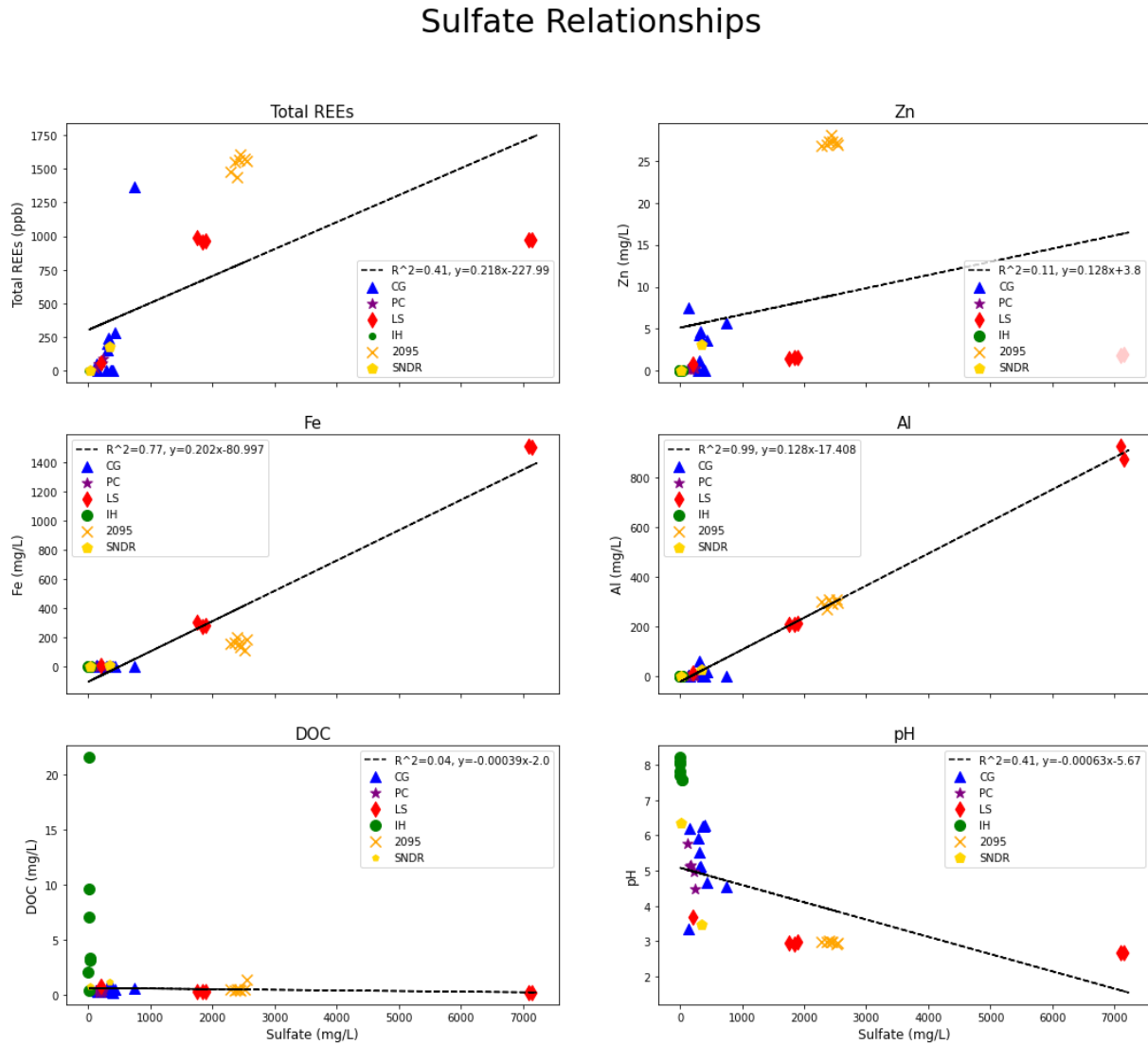


Figure 35. Sulfate relationships.

Generally, sulfate acts as a conservative tracer and can be helpful in comparing relationships to other water constituents (McKnight & Bencala, 1988, 1990; Verplanck et al., 1999). Comparison of sulfate relationships between all sites showed the only statistically significant relationship is

between Al and sulfate.

R-Studio Two-Sample T-Test Output

This test was used to determine if there is a statistically significant difference of the amount of REEs in flocculant dominated by Al vs. Fe.

Output:

$t = -3.0102$, $df = 18.37$, **p-value = 7.39×10^{-3}**

Alternative hypothesis: true difference in means is not equal to 0

95 percent confidence interval: -546.02445 -97.52152

Sample estimates:

Mean of x; Mean of y

57.35333; 379.12632

Table 3. Field and Single Water Measurements

Sample	Distance (km)	Easting	Northing	Temp °C	Conductivity (µS/cm)	pH	DOC ppm	Sulfate ppm
BC1	0	321916	4234092	12.4	248	7.77	1.756	4.1
BC2	0.4	321714	4234427	12.9	267	7.83	2.041	4.87
BC3	1.7	320755	4235076	19.4	426	7.7	9.647	5.01
BC4	2.13	320394	4235115	17.5	433	8.04	21.58	5.75
BC5	2.41	320131	4235188	17.4	434	8.22	7.05	5.04
C1	3.69	318858	4232037	15.5	187	7.58	3.161	26.51
C2	8.15	316556	4238497	16.9	188	7.56	3.301	26.14
DC	5.04	320787	4236540	15.1	257	8.1	0.4365	5.02
2095-1	0	427923	4379096	20.5	3.29	2.95	0.474	2391.86
2095-2	0.09	427859	4379056	20.6	3.53	2.99	0.4826	2436.09
2095-3	0.16	427804	4379027	22	3.65	2.99	0.4375	2366.35
2095-4	0.23	427756	4378980	21.2	3.66	3	0.4658	2402.34
2095-5	0.38	427635	4378894	19.2	3.62	2.98	0.4569	2285.40
2095-6	0.5	427525	4378923	18.4	3.71	2.94	1.346	2546.04
2095-7	0.6	427426	4378942	16.9	3.65	2.91	0.4691	2524.25

Sample	Distance (km)	Easting	Northing	Temp °C	Conductivity (µS/cm)	pH	DOC ppm	Sulfate ppm
BC1	0	321916	4234092	12.4	248	7.77	1.756	4.1
BC2	0.4	321714	4234427	12.9	267	7.83	2.041	4.87
BC3	1.7	320755	4235076	19.4	426	7.7	9.647	5.01
BC4	2.13	320394	4235115	17.5	433	8.04	21.58	5.75
BC5	2.41	320131	4235188	17.4	434	8.22	7.05	5.04
C1	3.69	318858	4232037	15.5	187	7.58	3.161	26.51
2095-8	0.67	427362	4378953	15.5	3.77	2.99	0.4438	2446.60
SN-DR		426073	4370708	7.5	1.034	3.71	0.718	227.50
SN		466089	4379696	8.8	0.993	3.47	0.8295	348.84
DR		426082	4379681	10.5	0.149	6.36	1.226	24.05
PC-PCT1	0	322127	4317666	6.1	471	4.48	0.4363	36.58
PCT-2	0.53	321652	4317802	7.1	362	5.13	0.4138	222.9211
PC1	0.72	321640	4317998	8.1	366	5.15	0.2436	235.29
PC2	0.9	321650	4318168	10.3	269	5.76	0.384	163.49
PC3	0.33	321827	4317785	10.9	124	6.36	1.514	165.24
PC4	0.36	321803	4317741	6.6	458	4.98	0.2291	112.9629
LS1	0	368597	4320780	6.7	6670	2.68	0.2692	7225.22
LS2	0.05	368548	4320800	12.7	6680	2.69	0.2215	7102.48
LS3	0.3	368383	4320984	15.1	7000	2.66	0.2467	7151.25
LS4	1.78	368174	4322395	9.8	2780	2.95	0.3039	1762.06
LS5	1.95	368158	4322544	10.2	2870	2.97	0.2957	1890.15
LS6	2.19	368166	4322786	11.3	2860	2.93	0.2642	1843.2
LS7	2.51	368383	4322923	9	469	3.7	0.7541	204.22
LF	2.28	368128	4322841	11.3	261	4.59	0.5682	165.11
CGS1-EAST	0.29	270423	4199953	4.7	1466	4.55	0.5988	135.18
CGS2-Mid	0.26	270381	4199984	6.8	572	5.92	0.2901	748.25
CG-MINE	0.07	270246	4199763	3.1	454	3.35	0.4454	294.48
CG1	0	270277	4199715	5.3	740	6.25	0.2926	379.75
CG2	0.06	270294	4199770	6.3	759	6.25	0.8958	362.95
CG-3	0.12	270293	4199829	5.6	713	6.28	0.2569	396.81
CG-4	0.26	270328	4199974	7	386	6.21	0.3066	147.68
GC-5	0.46	270410	4200157	8.8	668	5.53	0.3514	307.44
CG-6	0.95	270610	4200568	9.6	786	4.67	0.5134	427.51
CG-7	2.58	271910	4201471	10.4	677	5.11	0.7471	334.84
CG-8	3.54	272371	4201378	10.8	631	5.08	0.7486	309.05

Table 4. Water REE Concentrations

	ppb	ppb	ppb	ppb												
Sample	Ce	Pr	Nd	Sm	Eu	Gd	Tb	Dy	Ho	Er	Tm	Yb	Lu	Y	La	Total REEs
CG-MINE	12.9	2.0	8.4	2.2	0.9	2.7	0.4	1.8	0.3	0.6	0.1	0.4	0.0	6.8	7.7	47.3
CGS1-EAST	469.4	51.4	135.7	20.7	1.6	27.7	3.7	24.0	5.2	15.9	2.1	13.4	2.0	192.2	401.1	1366.2
CGS2-Mid	0.2	0.1	0.3	0.0	0.0	0.1	0.0	0.0	0.0	0.0	0.0	0.0	0.0	0.4	1.5	2.7
CG1	0.1	0.1	0.5	0.1	0.0	0.1	0.0	0.0	0.0	0.0	0.0	0.0	0.0	0.4	1.8	3.2
CG2	0.1	0.1	0.2	0.0	0.0	0.0	0.0	0.0	0.0	0.0	0.0	0.0	0.0	0.2	0.8	1.4
CG-3	0.1	0.0	0.1	0.0	0.0	0.0	0.0	0.0	0.0	0.0	0.0	0.0	0.0	0.1	0.6	1.0
CG-4	0.3	0.4	1.5	0.2	0.1	0.3	0.0	0.1	0.0	0.1	0.0	0.0	0.0	1.0	2.3	6.2
GC-5	38.4	6.2	16.8	2.5	0.3	3.5	0.4	2.8	0.6	1.8	0.2	1.2	0.2	24.6	56.5	155.8
CG-6	63.3	11.9	41.0	7.2	1.2	8.8	1.2	7.1	1.4	4.0	0.5	2.7	0.4	53.0	77.0	280.7
CG-7	53.3	11.0	39.9	7.1	1.3	8.4	1.1	6.5	1.3	3.6	0.4	2.4	0.3	47.5	62.6	246.7
CG-8	44.0	9.2	33.4	5.9	1.1	7.0	0.9	5.5	1.1	3.0	0.4	2.0	0.3	40.1	52.4	206.3
PCT-1	0.1	0.0	0.0	0.0	0.0	0.0	0.0	0.0	0.0	0.0	0.0	0.0	0.0	0.1	1.5	1.7
PCT-2	12.1	2.8	11.9	2.7	1.0	3.1	0.4	2.6	0.5	1.3	0.2	0.9	0.1	13.1	10.1	62.7
PC1	22.1	3.9	17.2	4.1	1.5	4.4	0.6	3.8	0.7	1.9	0.2	1.3	0.2	17.7	12.5	91.9
PC 2	9.5	2.2	9.2	2.1	0.8	2.4	0.3	2.0	0.4	1.0	0.1	0.7	0.1	10.0	8.0	48.6
PC 3	9.6	2.2	9.2	2.1	0.8	2.4	0.3	2.0	0.4	1.0	0.1	0.7	0.1	10.1	8.1	49.0
PC 4	4.4	1.0	4.1	0.8	0.3	1.0	0.1	0.8	0.1	0.4	0.0	0.2	0.0	4.5	4.1	21.9
LF	7.2	1.1	4.8	1.1	0.3	1.2	0.2	0.9	0.2	0.4	0.0	0.3	0.0	3.8	3.4	25.0
LS1	315.6	44.7	201.8	53.7	13.9	50.8	7.3	38.4	6.4	16.9	1.9	12.1	1.6	125.4	91.8	982.1
LS2	311.0	43.5	198.0	52.8	13.6	50.1	7.2	37.9	6.5	16.6	1.9	11.9	1.6	125.6	91.1	969.3
LS3	310.1	44.3	199.2	53.1	13.5	48.6	7.0	37.5	6.4	16.3	1.9	11.6	1.5	129.2	90.8	971.2
LS4	276.0	45.3	198.6	43.6	10.7	43.6	6.1	33.6	6.2	16.4	1.9	11.6	1.6	162.9	133.4	991.6
LS5	269.8	44.4	194.2	43.0	10.5	42.7	6.0	33.0	6.0	16.1	1.9	11.5	1.6	157.7	130.1	968.6
LS6	264.9	43.8	192.5	42.5	10.4	42.7	6.0	32.7	6.0	15.9	1.9	11.4	1.6	155.7	128.2	956.2

LS7	16.1	2.6	11.4	2.5	0.7	2.7	0.4	2.1	0.4	1.0	0.1	0.7	0.1	9.2	8.0	57.9
BC1	0.0	0.0	0.0	0.0	0.1	0.0	0.0	0.0	0.0	0.0	0.0	0.0	0.0	0.0	0.8	1.0
BC2	0.1	0.0	0.0	0.0	0.1	0.0	0.0	0.0	0.0	0.0	0.0	0.0	0.0	0.0	1.0	1.2
BC3	0.0	0.0	0.0	0.0	0.1	0.0	0.0	0.0	0.0	0.0	0.0	0.0	0.0	0.0	0.5	0.7
BC4	0.0	0.0	0.0	0.0	0.1	0.0	0.0	0.0	0.0	0.0	0.0	0.0	0.0	0.0	2.5	2.8
BC5	0.1	0.0	0.0	0.0	0.1	0.0	0.0	0.0	0.0	0.0	0.0	0.0	0.0	0.0	1.6	2.0
C1	0.1	0.0	0.0	0.0	0.0	0.0	0.0	0.0	0.0	0.0	0.0	0.0	0.0	0.1	0.1	0.3
C2	0.1	0.0	0.0	0.0	0.0	0.0	0.0	0.0	0.0	0.0	0.0	0.0	0.0	0.1	1.1	1.4
DC	0.1	0.0	0.0	0.0	0.1	0.0	0.0	0.0	0.0	0.0	0.0	0.0	0.0	0.0	0.3	0.7
DR-SN	17.6	3.9	20.3	5.0	1.1	6.0	0.9	5.6	1.1	3.0	0.4	2.2	0.3	33.0	11.1	111.6
SN	27.2	6.3	32.6	8.0	1.7	9.5	1.4	9.0	1.8	4.9	0.6	3.5	0.5	51.4	17.3	175.7
DR	0.0	0.0	0.0	0.0	0.0	0.0	0.0	0.0	0.0	0.0	0.0	0.0	0.0	0.1	0.0	0.2
2095-1	237.0	48.2	295.0	92.3	21.1	112.2	17.9	116.2	22.7	62.5	8.1	48.2	6.7	681.0	58.9	1827.9
2095-2	199.8	41.5	256.1	79.7	18.3	97.5	15.6	101.2	19.9	54.5	7.0	42.6	5.8	580.5	49.6	1569.7
2095-3	200.5	40.7	249.7	77.6	17.8	94.8	15.2	98.4	19.3	52.9	6.8	41.3	5.6	575.2	52.6	1548.5
2095-4	134.9	41.9	256.8	80.1	18.5	97.8	15.7	101.5	19.9	54.8	7.1	42.6	5.8	519.0	43.5	1439.9
2095-5	178.0	41.2	252.2	78.1	18.0	95.4	15.3	98.9	19.4	53.1	6.9	41.5	5.6	524.6	46.1	1474.3
2095-6	198.7	42.0	258.0	80.0	18.3	96.9	15.6	101.2	19.8	54.3	7.0	42.6	5.8	565.2	49.7	1555.1
2095-7	201.4	42.0	258.3	79.9	18.4	97.7	15.7	101.6	19.9	54.8	7.1	42.6	5.8	578.2	51.8	1575.2
2095-8	211.0	42.4	259.8	80.5	18.6	98.3	15.8	102.6	20.2	55.2	7.1	43.0	5.9	595.9	52.7	1609.0

Table 5. Water Trace Metal Concentrations

	ppb	ppb	ppb	ppb	ppb	ppb	ppb	ppb	ppm	ppm	ppm	ppm	ppm	ppm
Sample	Cd	Co	Ni	Pb	Mn	Cu	Zn	Al	Fe	Ca	Na	K	Mg	
CG-MINE	70.2	8.2	7.9	175.2	5321.2	2098.5	7451.9	5.6	9.1	13.8	0.7	0.8	2.0	
CGS1-EAST	12.0	35.7	69.8	0.3	166910.9	18.0	5755.1	0.1	0.0	19.5	3.6	3.0	2.9	
CGS2-Mid	0.1	0.0	0.7	0.1	190.8	0.7	45.4	10.2	0.0	20.5	1.6	0.4	2.6	
CG1	0.6	0.2	2.5	0.1	24.7	3.2	140.3	0.0	0.0	20.6	1.4	4.2	2.7	

CG2	0.3	0.0	1.5	0.1	17.4	1.1	94.4	0.0	0.0	20.6	1.5	4.5	2.7
CG-3	0.3	0.0	1.1	0.1	2.8	1.0	50.3	0.0	0.0	19.3	1.0	0.5	2.4
CG-4	2.1	0.0	2.0	0.4	95.4	5.6	386.3	0.2	0.0	20.5	1.4	0.5	2.7
GC-5	2.7	0.9	11.7	0.2	28329.9	6.2	1213.1	62.8	0.0	19.5	2.0	0.9	2.6
CG-6	14.4	5.1	24.1	0.5	52616.5	54.3	3698.6	18.9	0.0	18.6	2.0	1.1	2.7
CG-7	17.1	5.7	23.7	0.6	37938.5	43.5	4708.8	13.9	0.1	18.2	1.9	1.1	2.6
CG-8	14.9	5.0	20.5	0.9	33824.3	35.8	4247.9	10.2	0.2	19.0	2.1	1.1	2.6
PCT-1	0.3	0.1	0.2	0.7	26.7	3.8	44.5	0.0	0.0	14.7	0.8	0.2	1.5
PCT-2	1.9	2.9	14.8	1.2	448.0	255.6	259.0	1.5	0.0	19.8	1.6	0.5	1.9
PC1	2.4	7.1	32.6	8.4	644.3	444.6	256.0	4.8	0.0	19.5	1.8	0.6	2.7
PC 2	1.6	2.1	11.9	1.1	301.9	180.4	192.7	0.9	0.0	18.6	1.5	0.5	2.7
PC 3	1.6	2.1	11.6	1.1	287.7	172.6	186.9	0.9	0.0	18.6	1.4	0.4	2.7
PC 4	1.1	1.1	7.5	0.4	143.7	80.4	119.3	0.1	0.0	18.4	1.1	0.3	2.4
LF	0.8	19.4	27.0	0.3	128.3	130.9	705.6	10.7	10.9	14.4	1.6	0.6	2.4
LS1	22.1	908.1	1039.8	0.3	3121.9	42804.4	1921.6	900.3	1718.0	0.3	2.1	3.8	3.0
LS2	24.1	913.1	1044.4	2.9	3064.6	41913.4	1877.2	925.8	1512.6	0.2	1.9	3.7	3.0
LS3	22.7	942.3	1083.7	0.1	3203.8	43838.8	1964.6	873.8	1505.6	0.2	1.8	3.4	3.0
LS4	13.2	345.9	443.5	0.3	3826.5	10495.4	1518.2	208.1	301.0	7.1	3.0	1.1	3.0
LS5	12.9	330.6	424.7	0.3	3962.2	10830.6	1572.9	212.6	280.0	6.1	3.1	1.4	3.0
LS6	12.8	326.3	421.6	0.4	3844.4	10513.8	1525.2	209.6	270.7	6.0	3.1	1.6	3.0
LS7	1.1	25.0	34.4	0.3	159.9	265.6	802.9	15.4	3.8	13.5	1.7	1.4	2.5
BC1	0.0	0.0	0.1	0.6	15.9	1.5	1.9	0.0	0.0	15.0	3.8	2.0	2.5
BC2	0.0	0.0	0.2	0.6	19.8	2.4	7.3	0.0	0.0	15.5	3.9	2.5	2.5
BC3	0.0	0.1	0.0	0.5	77.0	1.7	2.2	0.0	0.0	18.3	4.1	4.1	2.6
BC4	0.0	0.1	0.0	0.5	39.8	1.4	1.0	0.0	0.0	18.6	4.1	4.3	2.7
BC5	0.0	0.1	0.5	0.5	5.2	2.4	10.2	0.0	0.0	18.5	4.2	4.3	2.6
C1	0.0	0.1	0.1	0.5	29.7	1.2	2.7	0.1	0.0	9.6	3.4	2.0	2.2
C2	0.0	0.2	0.1	0.6	38.2	2.5	3.4	0.1	0.0	10.3	3.5	2.2	2.3

DC	0.0	0.0	0.1	0.2	5.8	1.0	4.9	0.0	0.0	16.1	4.0	1.9	2.5
DR-SN	15.3	37.5	1.3	70.9	4436.4	63.2	1980.7	16.3	0.4	11.7	2.7	1.1	2.7
SN	24.0	57.4	2.1	110.1	7184.9	103.4	3188.0	25.4	3.6	9.9	3.0	1.2	2.8
DR	0.0	0.1	0.1	0.8	18.9	1.0	18.2	0.0	0.0	13.5	1.6	0.7	2.0
2095-1	365.2	887.6	1355.0	0.6	84551.9	967.3	31621.9	311.6	251.3	3.0	3.8	1.5	3.3
2095-2	317.4	748.5	1134.9	0.4	78197.9	858.3	28023.9	294.9	153.7	3.2	3.7	1.5	3.3
2095-3	309.4	734.8	1112.2	1.0	74888.0	814.6	26879.2	270.8	162.8	3.3	3.8	1.6	3.3
2095-4	321.4	622.5	712.5	0.2	73028.5	835.3	27309.5	308.3	203.6	3.0	3.7	1.3	3.3
2095-5	311.6	643.1	1027.1	0.2	75119.0	797.4	26798.2	299.3	158.2	3.0	3.8	1.4	3.3
2095-6	318.0	719.4	1098.1	0.4	75972.7	802.2	26956.0	294.8	187.7	3.4	3.7	1.4	3.3
2095-7	318.3	727.7	1127.7	0.4	73503.3	812.1	27185.6	306.9	112.8	3.6	3.7	1.3	3.3
2095-8	320.2	759.2	1160.6	0.7	77336.8	824.5	27348.2	290.7	135.5	3.2	3.7	1.7	3.3

Table 6. Flocculant Chemistry

						ppm	ppm	ppm	ppm	ppm	ppm	ppm	ppm	ppm	ppm	ppm	ppm	ppm	ppm
Sample	% C w/w	% N w/w	C:N mol	% Al w/w	Fe % weight	Total REES ppm	Al	Fe	Cd	Co	Cu	Mn	Ni	Pb	Zn	Ca	Na	Mg	K
CG-MINE	2.8	0.25	11.2	16.9	3.8	208.1	129000	55965	0.328	7.783	164.47	806.7	6.8	112.7	267.8	684.8	62.9	4544.6	932.3
CGS2-MID	8.6	0.47	18.3	7.93	3.3	223	178504.8	19585.6	0.313	4.308	135.48	590.2	4.6	104.7	293.8	502.8	47.2	2771.1	639.6
CG4	17.8	1.29	13.8	18.51	14.1	58.5	6566.6	335711.7	0.481	2.452	76.06	249.6	9.3	173	139.5	199.7	215.2	2708.3	3575.7
CG5	1.8	0.16	11.3	18.26	5.1	66.4	7993.5	155950.2	0.413	3.467	40.469	286.4	13.9	117.4	109.9	254.3	252.9	4344.7	3694.5
CG6	7.6	0.64	11.9	14.68	7	62.7	6085.4	85162.4	0.614	2.383	57.399	283.5	6.1	132.4	103.3	201.6	197.8	1538.9	2170.4
CG7	9.6	0.38	25.3	9.65	7.5	57	5284.2	345030.5	0.522	2.316	46.745	221.3	8.7	176	103.8	271.4	185.1	2729.7	3294.4
CG8	7.2	0.29	24.8	14.33	3.4	72.8	7987	121182.4	0.581	3.782	45.765	300.1	15.5	183.9	122.4	311.6	295.9	5016.9	5186.8
2095-3	15	0.58	25.9	13.78	41.4	6.5	5668.3	21945.2	0.273	0.346	53.708	260.1	0.7	212.9	20.2	80.9	66.5	309.2	268.2
2095-4	3.6	0.18	20.0	15.38	21.3	462.9	203935	31487	0.405	12.926	97.172	1837.1	11.4	246.9	632.4	2150.8	288.1	9156.3	2428.7

2095-5	5	0.26	19.2	6.75	9.1	1119.2	88933.5	59380.3	3.793	11.065	2409.764	1250.2	10.7	341.4	2417.8	1675.6	234.6	6044.6	1572
2095-6	6.2	0.27	23.0	19.44	58.6	1148	184901.4	22466.4	0.214	6.277	113.692	585.7	5.2	87.2	378.6	1272.7	62.1	3699.5	857.7
2095-7	4.8	0.24	20.0	13.95	20.2	215.9	81130.8	34987.4	0.408	12.311	136.384	1135.4	8.2	158.1	305.6	962.8	72.2	6728.3	1239.5
LS1	8	0.64	12.5	18.36	115.4	33.4	183278.1	92688.1	0.29	0.542	447.41	29.5	3	18.3	23.2	262.6	57.8	318.5	374.6
LS4	15.6	0.27	57.8	13.87	8.9	83.6	233564.7	4777	0.121	0.628	506.863	42.1	2.5	14.4	38.2	206.7	32.3	529.3	240.2
LS5	10	0.24	41.7	7.49	21.7	50.9	235107.7	15806.7	0.068	0.771	408.126	29.7	4.4	19.6	26.4	227.8	15.4	513.1	84.6
LS6	2.8	0.11	25.5	19.39	65.2	74.9	232043.6	2466.4	0.109	0.695	468.738	77	1.6	11.6	29.6	236.5	24.4	247.7	117
LS7	10.4	0.36	28.9	13.27	134.4	876.5	218089.2	3267.7	0.486	0.859	2674.015	67.4	4.5	51.4	157.8	355.6	17.6	290	324.2
LF	14.8	0.63	23.5	18.79	16.9	15.5	4675.1	604367.5	0.127	1.677	64.106	54.4	2.8	7.2	15.4	290.4	46.3	503	618.8
PCT2	3.6	0.14	25.7	21.82	4.2	233	178994.3	35614.2	0.542	1.354	264.524	112.6	4.2	106.4	256.5	348.9	146.1	271	76
PC2	8.6	0.26	33.1	14.85	1	330.5	153400.5	42416.8	1.039	4.183	316.227	389	9.9	148.8	433.2	661.6	206.6	905.3	250.3
PC3	6.4	0.21	30.5	18.23	0.7	462.1	201863.5	67047.6	1.364	4.768	406.426	537	10.9	176.4	654.4	847.2	917.5	899.6	310.8
PC4	17.8	0.48	37.1	16.9	0.8	425.6	173344	33477.9	1.228	2.972	421.554	288.8	10.5	145.2	583.4	794.8	391.2	593.2	184.1
SN A	33	0.76	43.4	12.9	8.5	79.6	210729	20980.4	0.523	1.669	108.887	152.2	2.9	58	85.6	211.4	111.1	480.6	170.5
SN B	35.2	0.83	42.4	13.56	7.7	58	10992.3	577882.3	0.287	1.056	41.921	96.8	3.4	33.1	53.1	151.2	47.6	542	451.4
SN C	33.2	0.74	44.9	12.45	3.3	42.5	5494.6	705737.5	0.203	0.807	28.525	72.4	2.2	17.3	36.8	102.4	45.9	219.3	231.8
SN D	10	0.37	27.0	12.73	6.1	67.9	12921.4	678726	0.375	0.677	49.61	70.1	2.3	49.4	28.8	96.5	85.1	300.5	348.6
DR-SN1	20	0.64	31.3	21.46	119.5	10	6397.4	616131.2	0.162	4.23	153.075	39.6	5.8	1.8	13.1	96	29.1	565.9	308.7
DR-SN2	24.8	0.73	34.0	30	172	41.2	7697.8	50313	0.137	4.07	89.662	271.3	4.3	15.7	63	515.3	112.6	2418.2	2377.8
DR-SN3	24.8	0.61	40.7	15.78	57.2	11.2	4114.7	297359.9	0.137	0.908	120.361	40.3	2	9.6	12.4	163	55.8	316.7	545.6
DR-SN4	14	0.4	35.0	11.23	77.9	21.1	9978.1	376238.7	0.158	0.386	221.601	52.4	0.5	6.2	5.7	134.5	22.5	217.8	106.6

Table 7. Cerium Anomaly Standard Values for PAAS and PPREE1

	Taylor and McLennan (1985)	Verplanck (1999)
Element	PAAS (ppb)	PREE1 (ppb)
La	38000	80.40
Ce	80000	161.20
Pr	8900	21.20
Nd	32000	92.30
Sm	5600	20.30
Eu	1100	5.95
Gd	4700	23.80
Tb	770	3.65
Dy	4400	22.00
Ho	1000	4.43
Er	2900	11.90
Tm	400	1.48
Yb	2800	8.2
Lu	430	1.12

Table 8. Calculated Values for Site Ce* Standardization

Sample	Pr ppb	La ppb	Ce ppb	Normalized PR	Normalized La	Normalized Ce	Ce*
CG1	0.134	1.761	0.070	0.003	0.004	0.000	0.042
CG2	0.052	0.767	0.069	0.001	0.002	0.000	0.100
CG-MINE	1.960	7.705	12.929	0.038	0.019	0.028	0.960
CG-3	0.037	0.561	0.058	0.001	0.001	0.000	0.116
CG-4	0.375	2.251	0.348	0.007	0.006	0.001	0.115
GC-5	6.168	56.450	38.378	0.120	0.141	0.082	0.627
CGS1-EAST	51.357	401.141	469.421	1.000	1.000	1.000	1.000
CGS2-Mid	0.108	1.459	0.185	0.002	0.004	0.000	0.137
CG-6	11.873	77.007	63.251	0.231	0.192	0.135	0.637
CG-7	10.961	62.585	53.279	0.213	0.156	0.113	0.614
CG-8	9.152	52.391	44.032	0.178	0.131	0.094	0.607
Highest Site	Pr ppb	La ppb	Ce ppb				
CGS1 East	51.357	401.144	469.421				

Sample	Pr ppb	La ppb	Ce ppb	Normalized PR	Normalized La	Normalized Ce	Ce*
PC1	3.87	12.52	22.05	1	1	1	1
PCT-1	0.010	1.48	0.052	0.003	0.118	0.002	0.039
PCT-2	2.76	10.12	12.06	0.712	0.808	0.547	0.719
PC 2	2.15	8.01	9.47	0.556	0.640	0.430	0.719
PC 3	2.16	8.06	9.56	0.557	0.643	0.433	0.722
PC 4	0.98	4.09	4.40	0.252	0.327	0.200	0.690
Highest Site	Pr ppb	La ppb	Ce ppb				
PC1	3.87	12.52	22.05				
	Pr ppb	La ppb	Ce ppb	Normalized PR	Normalized La	Normalized Ce	Ce*
LS1-AT	44.66	91.76	315.55	1.000	1.000	1.000	1.000
LS2-AT-pond	43.51	91.08	310.98	0.974	0.993	0.986	1.002
LS3-BTT	44.28	90.78	310.14	0.992	0.989	0.983	0.992
LS4-BT	45.31	133.38	275.98	1.015	1.454	0.875	0.709
LS5-BT	44.44	130.11	269.82	0.995	1.418	0.855	0.709
LS6-BT-PCLF	43.84	128.21	264.93	0.982	1.397	0.840	0.706
LS-PC	2.59	8.03	16.08	0.058	0.088	0.051	0.701
LF	1.08	3.40	7.21	0.024	0.037	0.023	0.746
Highest Site	Pr ppb	La ppb	Ce ppb				
LS2	44.66	91.76	315.55				
	Pr ppb	La ppb	Ce ppb	Normalized PR	Normalized La	Normalized Ce	Ce*
BC1	0.00	0.84	0.04	0.000	0.009	0.000	0.029
BC2	0.01	1.01	0.05	0.000	0.011	0.000	0.030
BC3	0.00	0.52	0.01	0.000	0.006	0.000	0.012
BC4	0.00	2.55	0.02	0.000	0.028	0.000	0.005
BC5	0.01	1.63	0.07	0.000	0.018	0.000	0.023
C1	0.01	0.06	0.06	0.000	0.001	0.000	0.485
C2	0.01	1.15	0.08	0.000	0.012	0.000	0.038
D1	0.01	0.34	0.08	1.000	1.000	1.000	1.000
Highest Site	Pr ppb	La ppb	Ce ppb				
D1	0.01	0.34	0.08				
2095	Pr ppb	La ppb	Ce ppb	Normalized PR	Normalized La	Normalized Ce	Ce*

1	48.17	58.91	236.96	1.00	1.00	1.00	1.00
2	41.51	49.63	199.76	0.86	0.84	0.84	0.99
3	40.69	52.64	200.53	0.84	0.89	0.85	0.97
4	41.88	43.54	134.91	0.87	0.74	0.57	0.71
5	41.15	46.05	178.00	0.85	0.78	0.75	0.92
6	42.04	49.69	198.71	0.87	0.84	0.84	0.98
7	42.03	51.77	201.43	0.87	0.88	0.85	0.97
8	42.42	52.67	211.04	0.88	0.89	0.89	1.00
Highest Site	Pr ppb	La ppb	Ce ppb				
1	48.17	58.91	236.96				
SN-DC Confluence	Pr ppb	La ppb	Ce ppb	Normalized PR	Normalized La	Normalized Ce	Ce*
SN-DC	3.94	11.09	17.64	0.62	0.64	0.65	1.03
SN	6.35	17.31	27.23	1.00	1.00	1.00	1.00
DC	0.01	0.05	0.03	0.00	0.00	0.00	0.58
Petach SN	5.615	11.5	25.45	0.88	0.66	0.93	1.21
Petach DC	0.046	0.1095	0.155	0.01	0.01	0.01	0.84
Highest Site	Pr ppb	La ppb	Ce ppb				
1	6.35	17.31	27.23				

Table 9. Cerium anomaly all methods for water and flocculant

Site	Water Ce*			Floc Ce*
	PAAS	PPREE	Site Ce*	PAAS
CG-MINE	0.764	0.852	0.960	1.4335
CGS1-EAST	0.719	0.786	1.000	
CGS2-WEST	0.091	0.099	0.137	0.4528
CG1	0.028	0.031	0.042	
CG2	0.066	0.071	0.100	
CG-3	0.076	0.082	0.116	
CG-4	0.086	0.094	0.115	0.2783
GC-5	0.440	0.479	0.627	0.63
CG-6	0.471	0.517	0.637	0.7075
CG-7	0.463	0.510	0.614	0.6502
CG-8	0.457	0.504	0.607	0.568
PC1	0.721	0.808	1.000	

PCT-1	0.032	0.034	0.039	
PCT-2	0.523	0.584	0.719	0.5572
PC 2	0.523	0.584	0.719	0.5338
PC 3	0.526	0.587	0.722	0.5618
PC 4	0.507	0.564	0.690	0.4378
LF	0.854	0.959	0.746	0.7383
LS1	1.061	1.205	1.000	1.018
LS2	1.067	1.211	1.002	
LS3	1.053	1.196	0.992	
LS4	0.802	0.902	0.709	1.3102
LS5	0.801	0.901	0.709	0.8217
LS6	0.798	0.897	0.706	0.8139
LS7	0.801	0.899	0.701	0.901
BC1	0.046	0.049	0.029	
BC2	0.048	0.051	0.030	
BC3	0.020	0.021	0.012	
BC4	0.009	0.009	0.005	
BC5	0.038	0.040	0.023	
C1	0.624	0.687	0.485	
C2	0.062	0.065	0.038	
D1	0.203	0.216	1.000	
2095-1	0.851	0.978	1.000	
2095-2	0.837	0.962	0.989	
2095-3	0.841	0.966	0.974	1.038
2095-4	0.576	0.665	0.708	1.0107
2095-5	0.763	0.879	0.918	1.0098
2095-6	0.824	0.948	0.977	0.9863
2095-7	0.828	0.951	0.971	1.0087
2095-8	0.858	0.986	1.004	
SN-DC	0.601	0.676	1.028	
SN	0.582	0.656	1.000	
DC	0.368	0.406	0.584	
SN-A (1980)				0.8285
SN-B (1980)				0.8032
SN-C (1980)				0.8498
SN-E (1980)				0.831
SN-F (1980)				0.7878
DR-SN 1				0.6916
DR-SN 2				0.6765

DR-SN 3				0.6399
DR-SN 4				0.7513

Table 10. Fluorescence Index

Sample	FI	Peak Wavelength between 470 and 520
PC1	1.792	490
PCT1-lake	1.485	492
PCT2	1.758	492
PC2	1.651	490
PC3	1.725	492
PC4	1.767	370
IH-D1	1.564	492
IH-C1	1.852	492
IH-C2	1.545	492
IH-BC1	1.558	492
IH-BC2-2	1.550	492
IH-BC3	1.591	492
IH-BC4	1.611	492
IH-BC5	1.609	492
2095-1	1.811	476
2095-2	1.888	476
2095-3	1.884	478
2095-4	1.876	478
2095-5	1.771	492
2095-6	1.837	478 and 492
2095-7	1.824	492
2095-8	1.752	492
DR-SN	1.346	492
SN	1.244	492
DR	1.109	492
CG1	1.113	472
CG2	1.286	470
CGMine	0.903	470
CG3	1.207	472

Sample	FI	Peak Wavelength between 470 and 520
PC1	1.792	490
PCT1-lake	1.485	492
PCT2	1.758	492
PC2	1.651	490
PC3	1.725	492
PC4	1.767	370
IH-D1	1.564	492
IH-C1	1.852	492
CG4	1.195	472
CGS1	1.086	472
CGS2	1.140	472
CG5	1.195	472
CG6	1.133	472
CG7	1.159	472
CG8	1.149	472
LS1	<i>-1.081</i>	IRON INTERFERENCE
LS2	<i>3.160</i>	
LS3	<i>1.404</i>	
LS4	1.894	472
LS5	1.827	472
LS6	1.315	470
LS7	1.794	472
LF	1.191	472